Fault Rheology: *Constraints from laboratory measurements on core samples from deep drilling into fault zones*

San Andreas Fault Observatory at Depth (SAFOD)

Sheryl Tembe, Teng-fong Wong (SUNY Stony Brook); *David Lockner, Diane Moore, Carolyn Morrow, John Solum* (USGS Menlo Park)

Taiwan Chelungpu-fault Drilling Project (TCDP)

Natalie Chen, Laurent Louis, Sheryl Tembe, Teng-fong Wong (SUNY Stony Brook); *David Lockner, Carolyn Morrow* (USGS Menlo Park); *Sheng-Rong Song, Li-Wei Kuo* (NTU); *Christian David, Phillipe Robion* (Cergy-Pontoise); *Wenlu Zhu* (WHOI)

- frictional strength
- velocity dependence of friction
- permeability and poromechanical properties
- dimension of the zone of dynamic weakening

San Andreas Fault Observatory at Depth (SAFOD)

The central scientific objective of SAFOD is to directly measure the physical and chemical processes that control deformation and earthquake generation within an active plate-bounding fault zone.

(*Zoback et al.*, AGU Fall Meeting 2005)

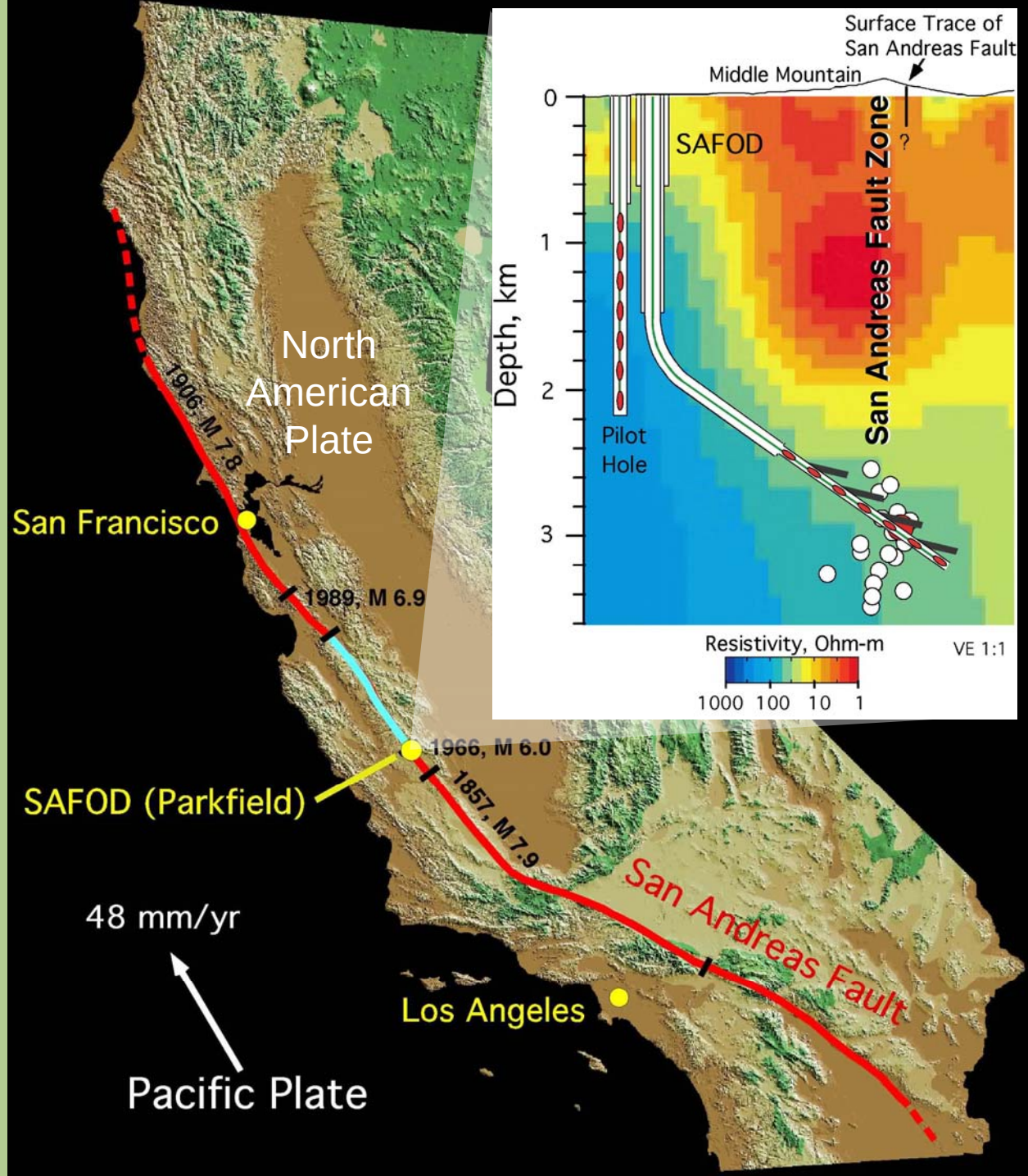

SAFOD Phase 1 Drilling: June - October 2004

(Pilot Hole drilled summer of 2002)

Phase 1: Rotary Drilling to 2.5 km

Drilled 12-1/4" hole to 2.5 km, while collecting continuous drill cuttings and carrying out mud gas analyses.

Below 1.5 km, steered hole toward target earthquakes (deviation 55°).

Conducted wireline geophysical logging in open hole (electrical and ultrasonic imaging, density, porosity, resistivity, dipole sonic, geochemical, temperature, etc.)

After setting casing, obtained 20 m of 4" diameter core at 1.5 and 2.5 km. Conducted permeability tests, fluid sampling and hydrofracs in core holes.

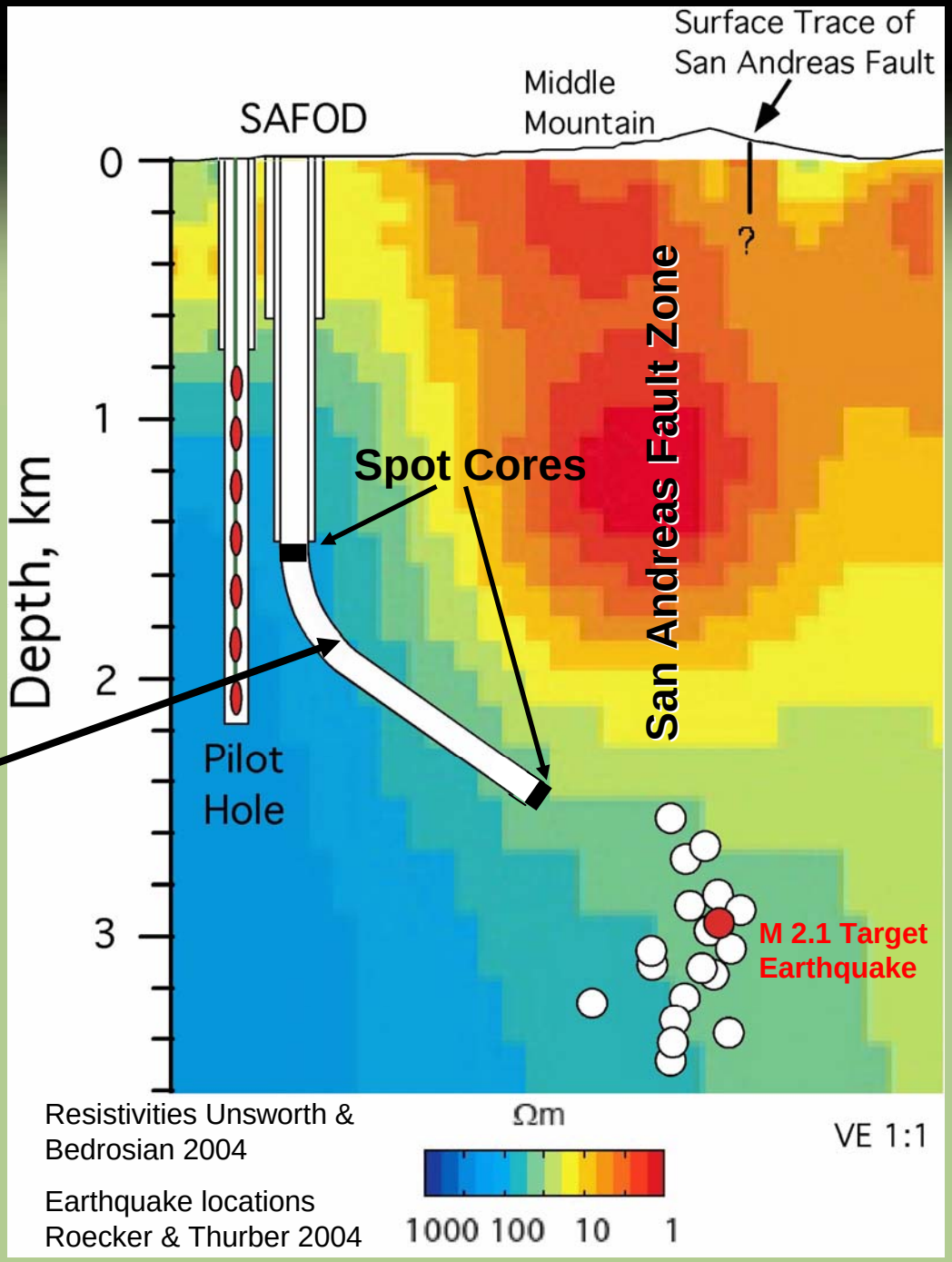

SAFOD Phase 2 Drilling: June - September 2005

<u>Phase 2: Drilling Through Fault Zone</u>

Drilled inclined 8-1/2" hole from 2.5 to 3.1 km.

Conducted extensive real-time cuttings and mud gas analyses while drilling across the fault zone.

Conducted comprehensive logging while drilling and wireline geophysical logging in open hole.

Collected 52 small (0.75" dia. x 1") side-wall cores in open hole.

After setting casing, collected 4 m of 2.6" dia. spot core at 3.1 km and carried out hydrofrac in core hole.

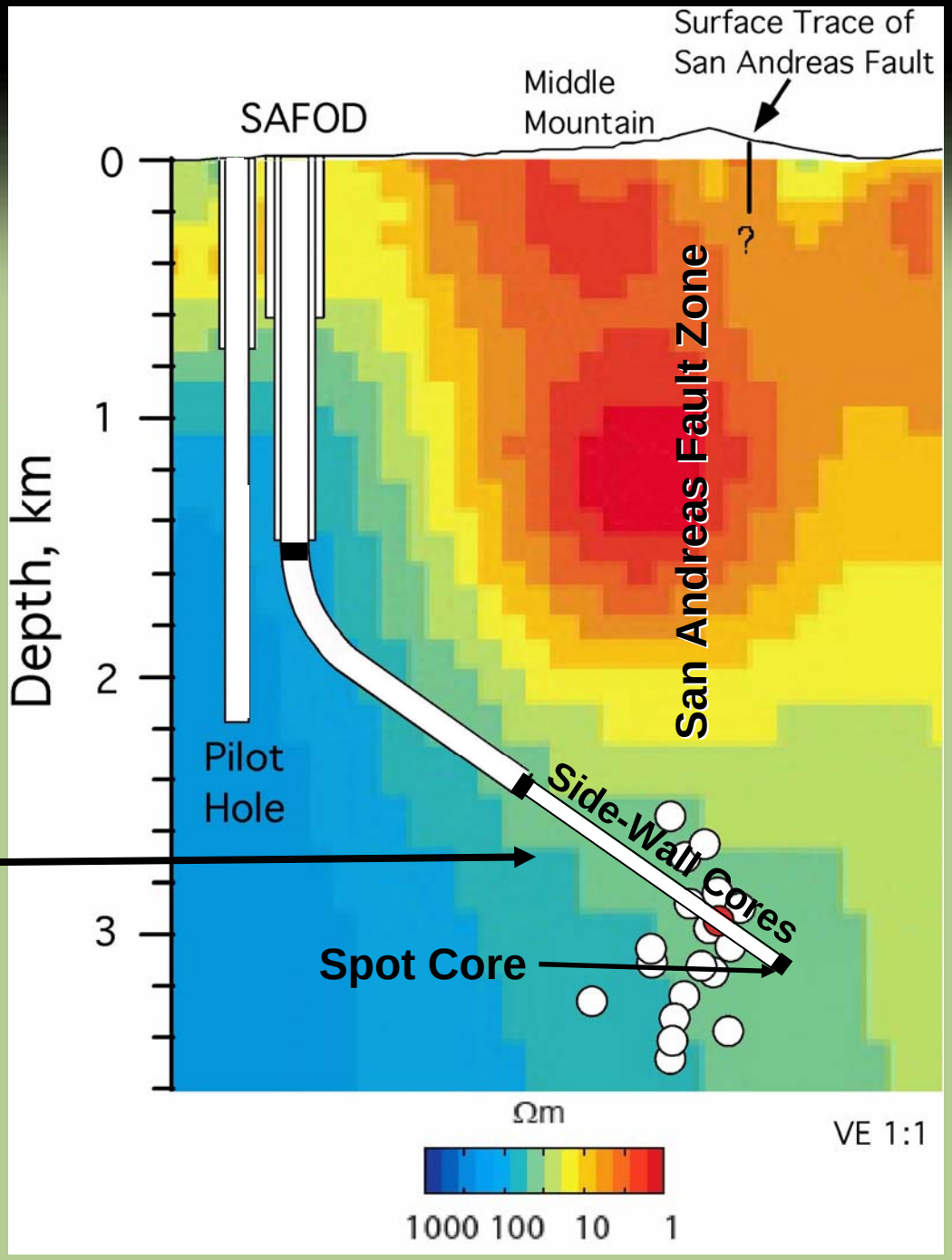

Pre-Drilling Geologic Model

Based upon geologic mapping, pilot hole studies, seismic imaging (natural earthquakes and active source) and potential-field studies (MT, gravity, magnetics)

Modified as a result of drilling:

- Vertical part of SAFOD encountered Salinian granitic basement as expected.
- But, sedimentary rocks encountered starting 210 m NE of drill site and persisted to bottom of hole at vertical depth of 3.1 km (4.0 km MD).

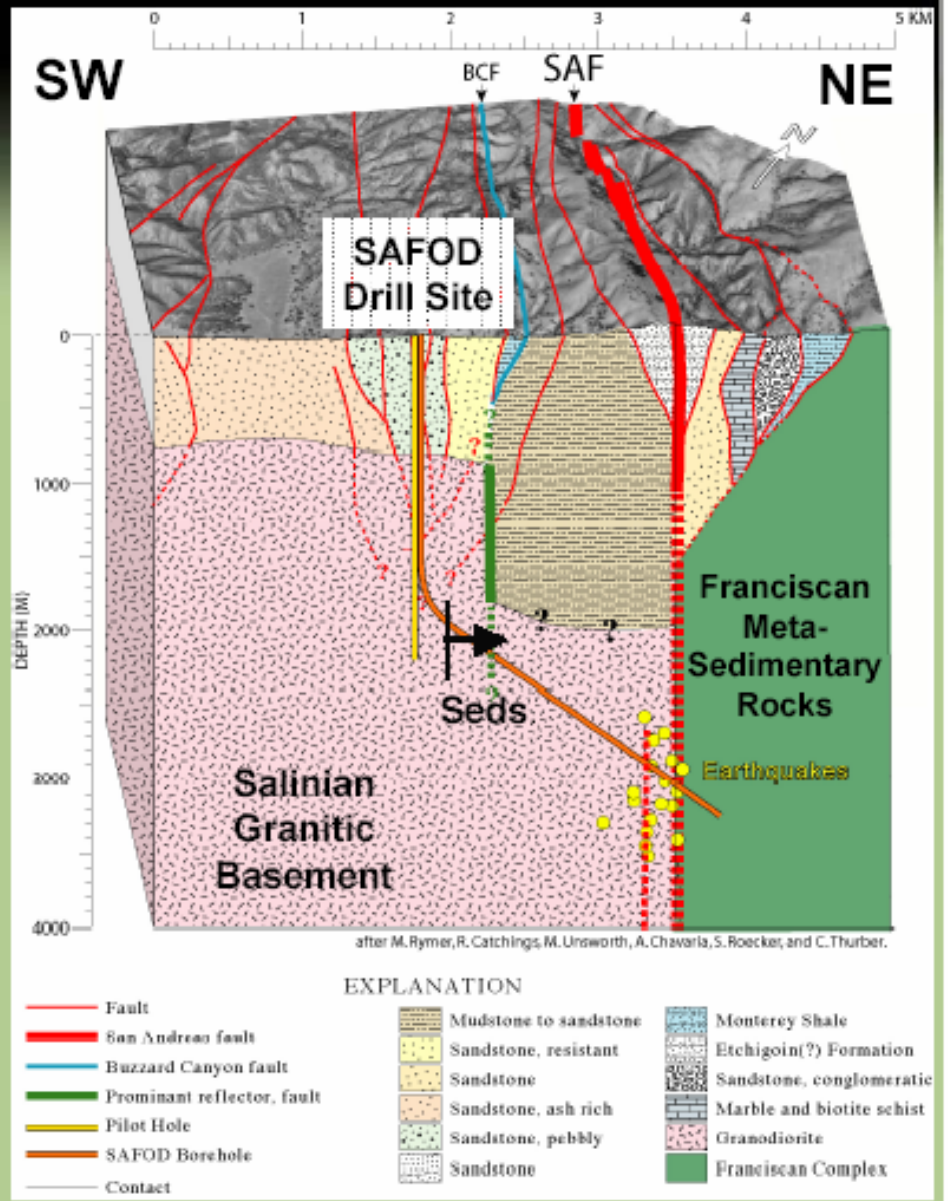

(*Hickman et al.*, AGU Fall Meeting 2005)

Post-Drilling Geologic Model

(from Draper et al., Evans et al., Barton et al., this session)

Long-term geologic manifestation of SAF is contact between Tertiary arkosic sandstone/ conglomerate and Cretaceous siltstone/shale (probably Great Valley Sequence, based on fossil assemblages and lack of high-pressure minerals)

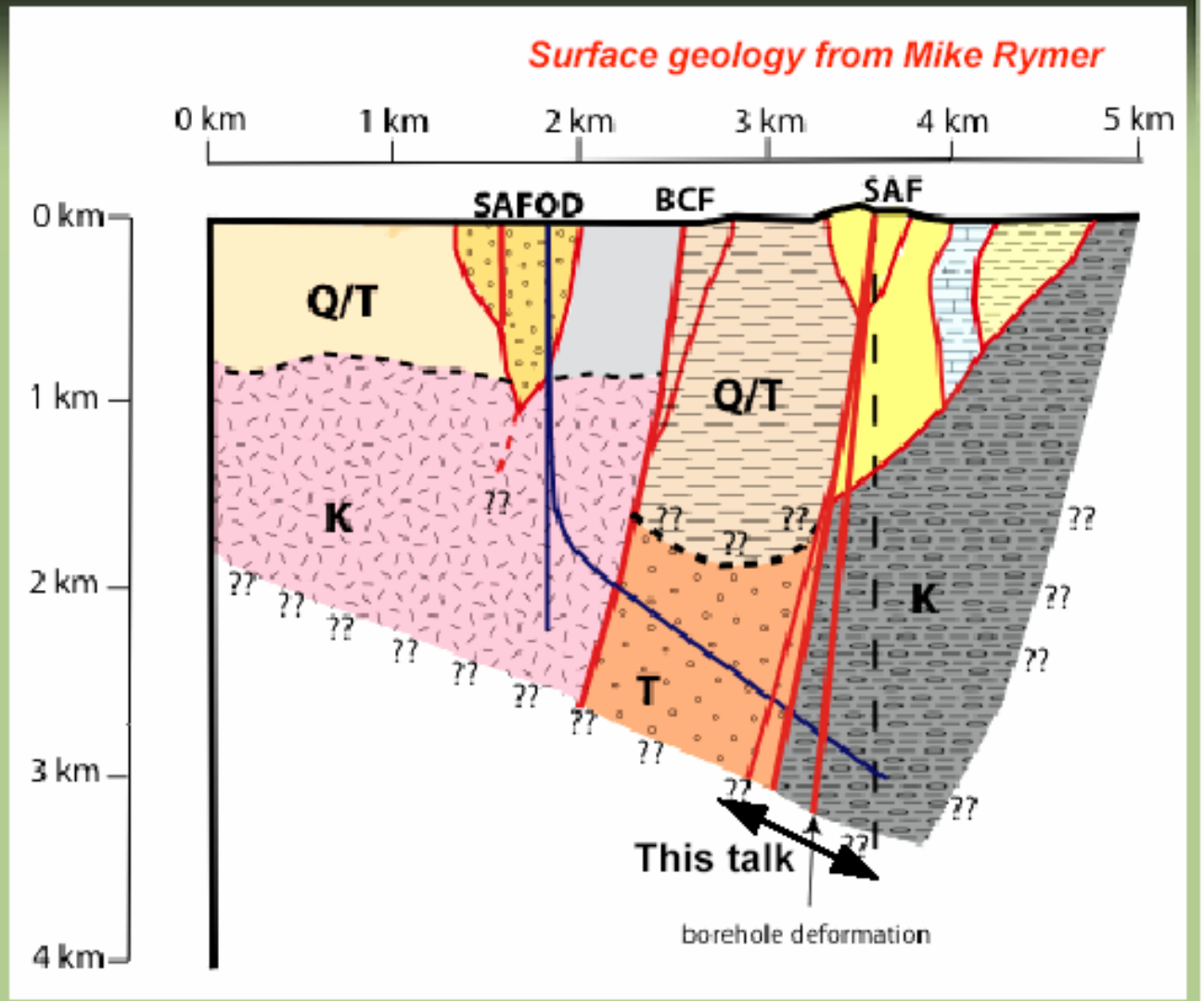

Samples collected to date:

- 3 spot cores
- 52 Sidewall cores 3081 - 3953 m MD, each ~1-3 cm^3
- Cuttings from entire length of the 3.9 km drillhole

(*Tembe et al.*, 2006)

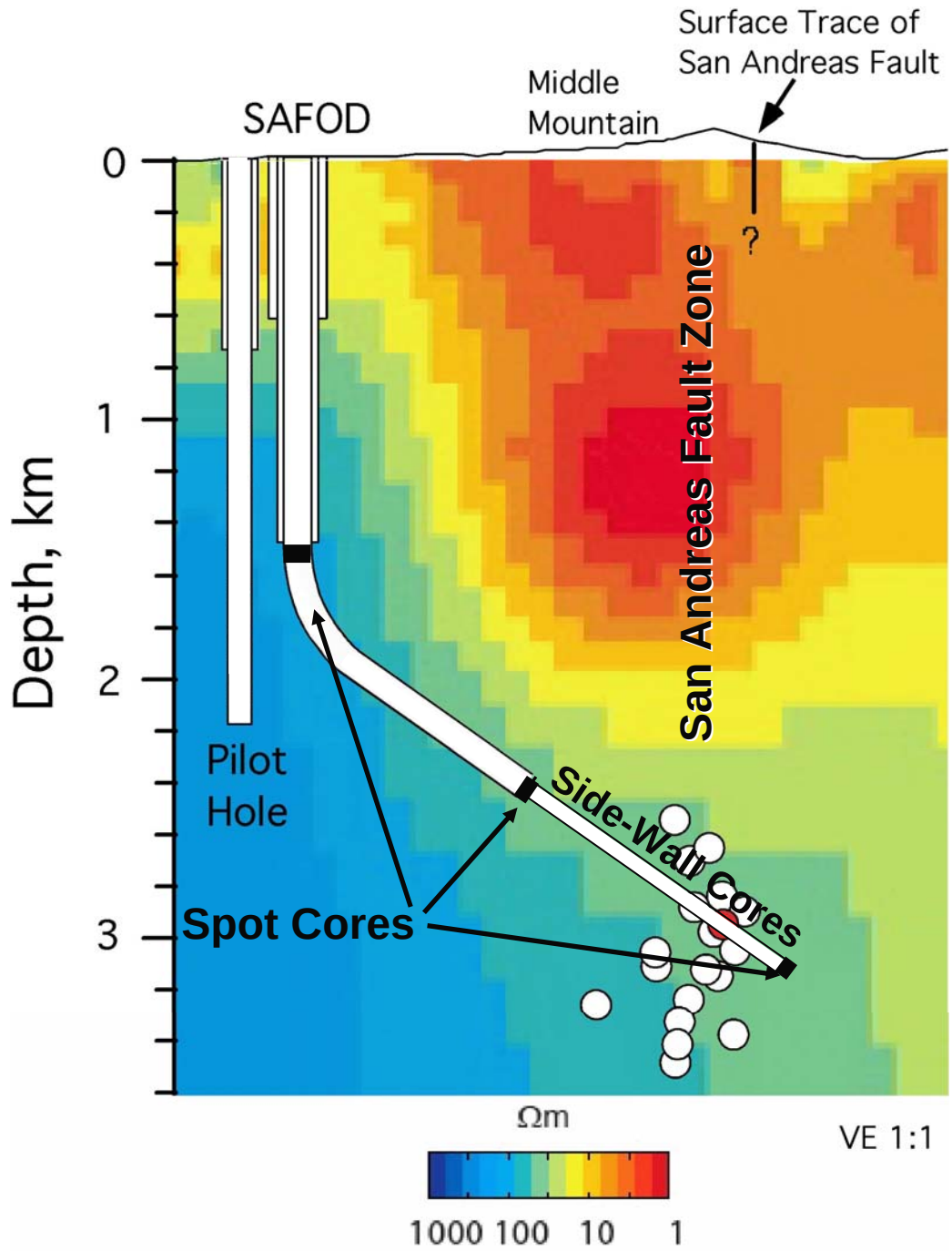

Sample selection

1890-3991 m MD

- Lithologic contacts
- Prominent shear zones including candidates for the SAF
- Cored sections

- Mixing (0.3-3 m intervals)
  - Bentonite drilling mud
  - Lost formation clays

Samples were washed, crushed and sieved to obtain particle sizes of <149 microns

Sliding Friction Tests

- Triaxial configuration
- Sample assembly
  - 30° saw-cut sandstone/granite forcing blocks
  - 1 mm thick gouge layer
- Constant normal stress and pore pressure
  - σ_n = 11 and 41 MPa; p_p = 1 MPa
  - Deionized water as pore fluid
- Velocity
  - Axial displacement rates of 0.01 to 1 μm/s corresponding to slip rates of 0.115 to 1.15 μm/s

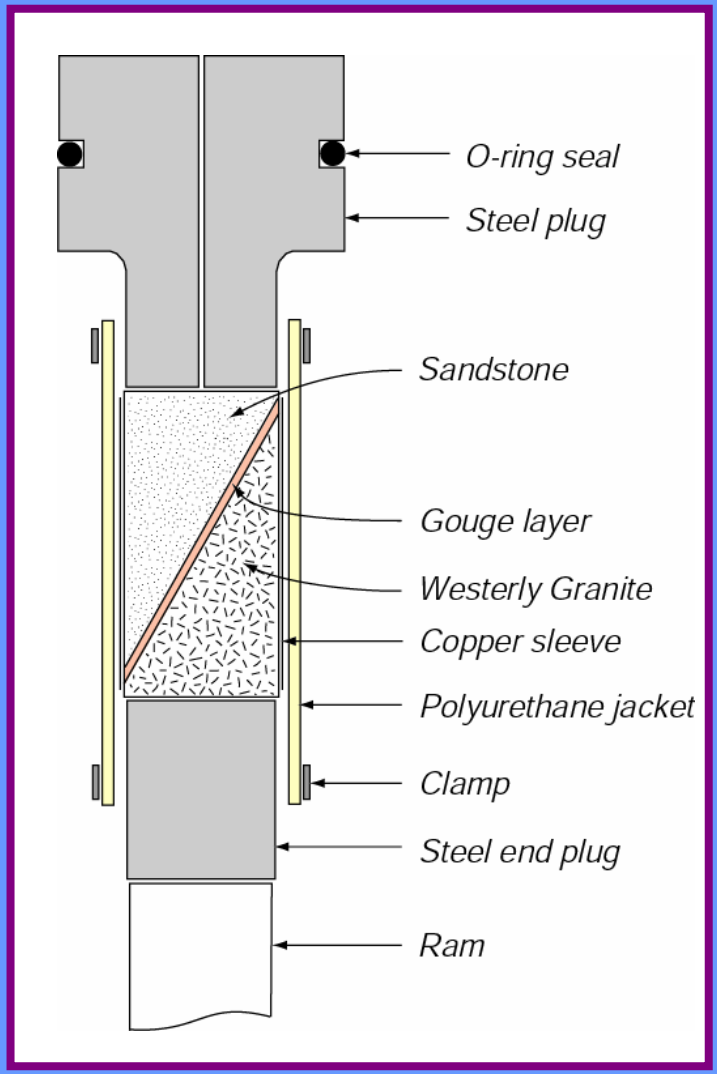

Cuttings 2377-2713 m MD

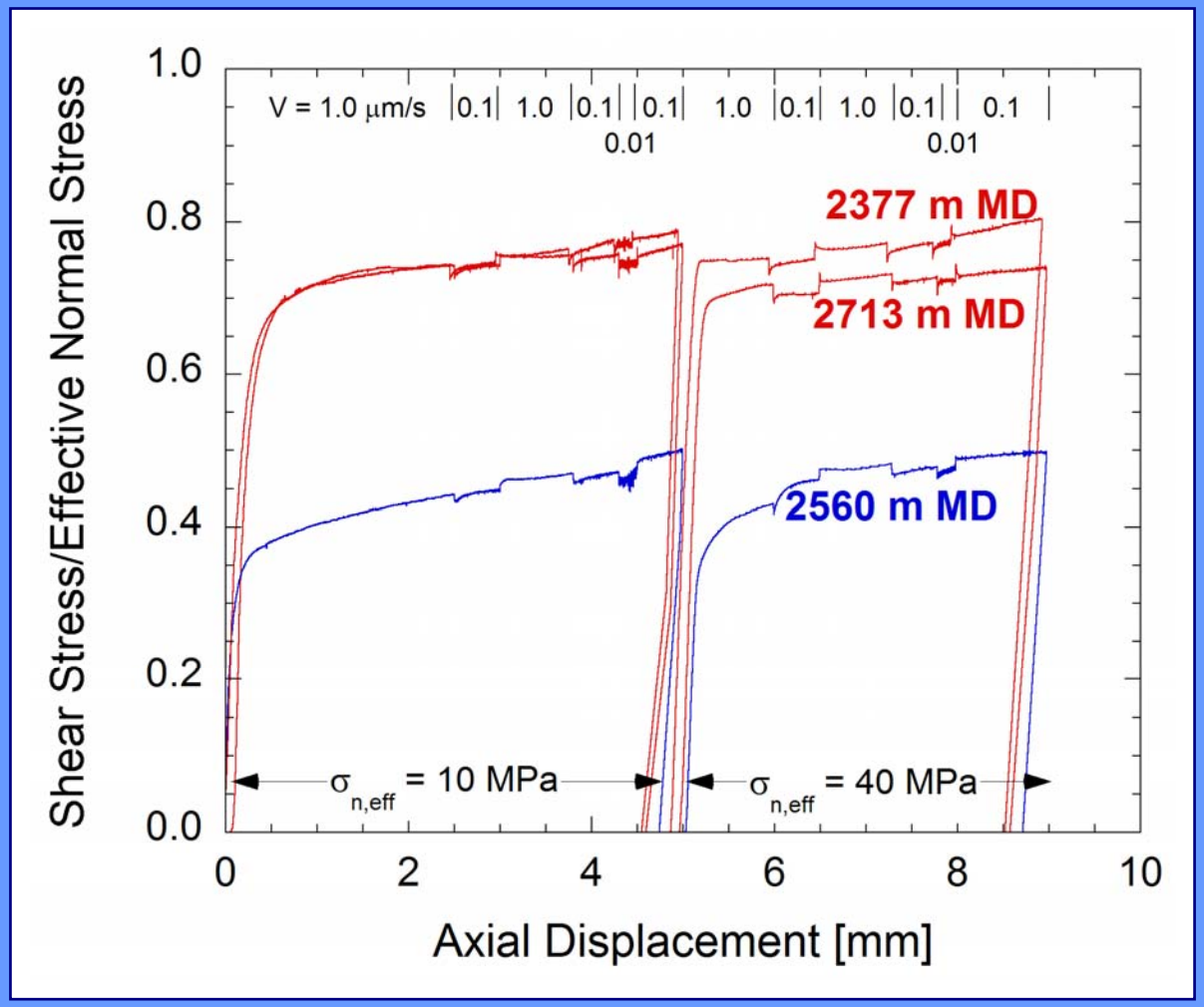

General observations:

- Frictional strength shows modest positive pressure dependence
- Stable sliding behavior
- Velocity strengthening
- Overall slip hardening

Shear zone must be several meters thick to be detected from cuttings

Core Samples SAFOD MH-ST1

Sliding tests on drill core samples:

3991 m MD

3067 m MD

3066 m MD

3056 m MD

Drill Core vs Cuttings

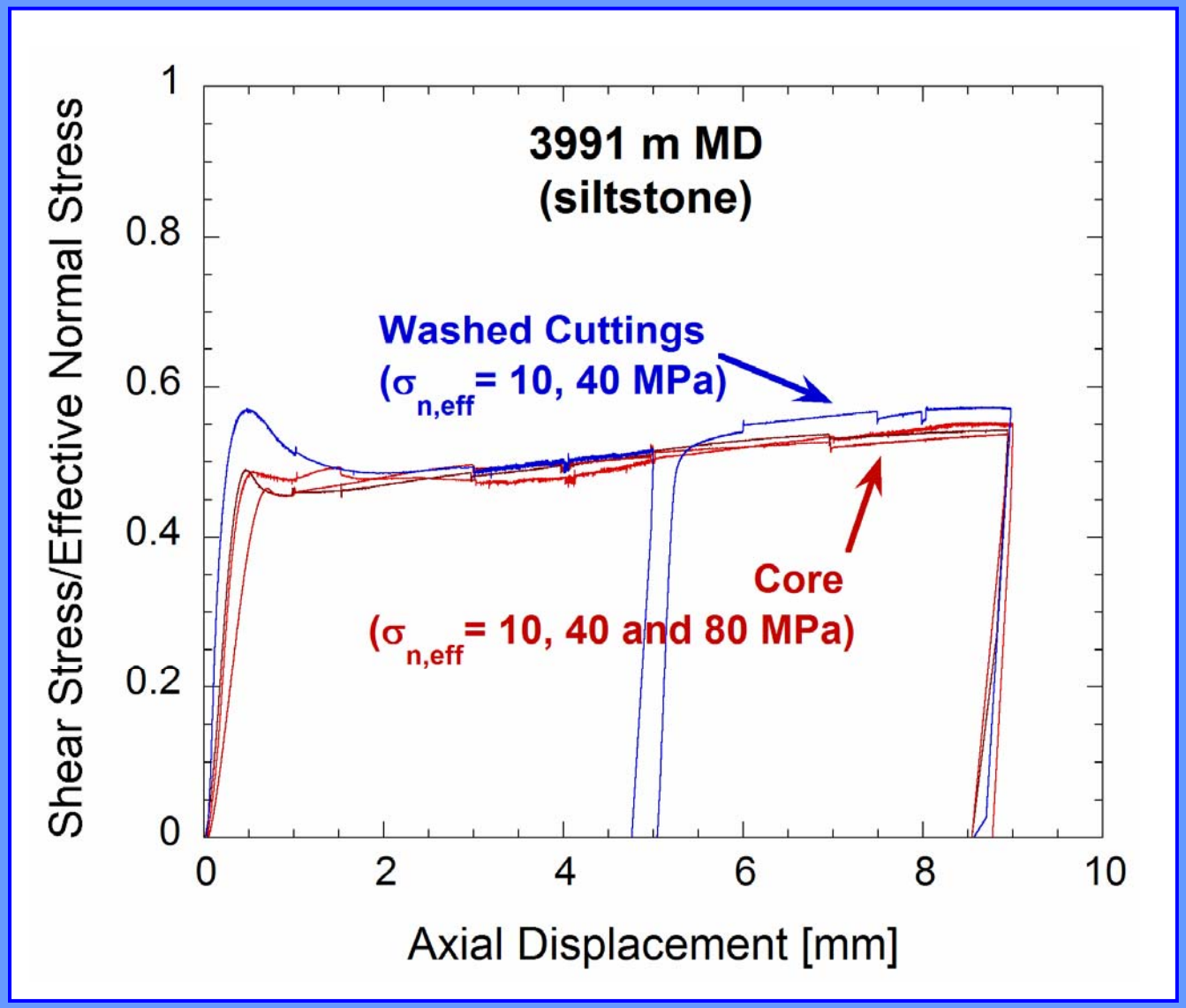

Prominent Faults Identified During Phase 2

(phys. props., bedding, drilling rate, cuttings mineralogy, gas)

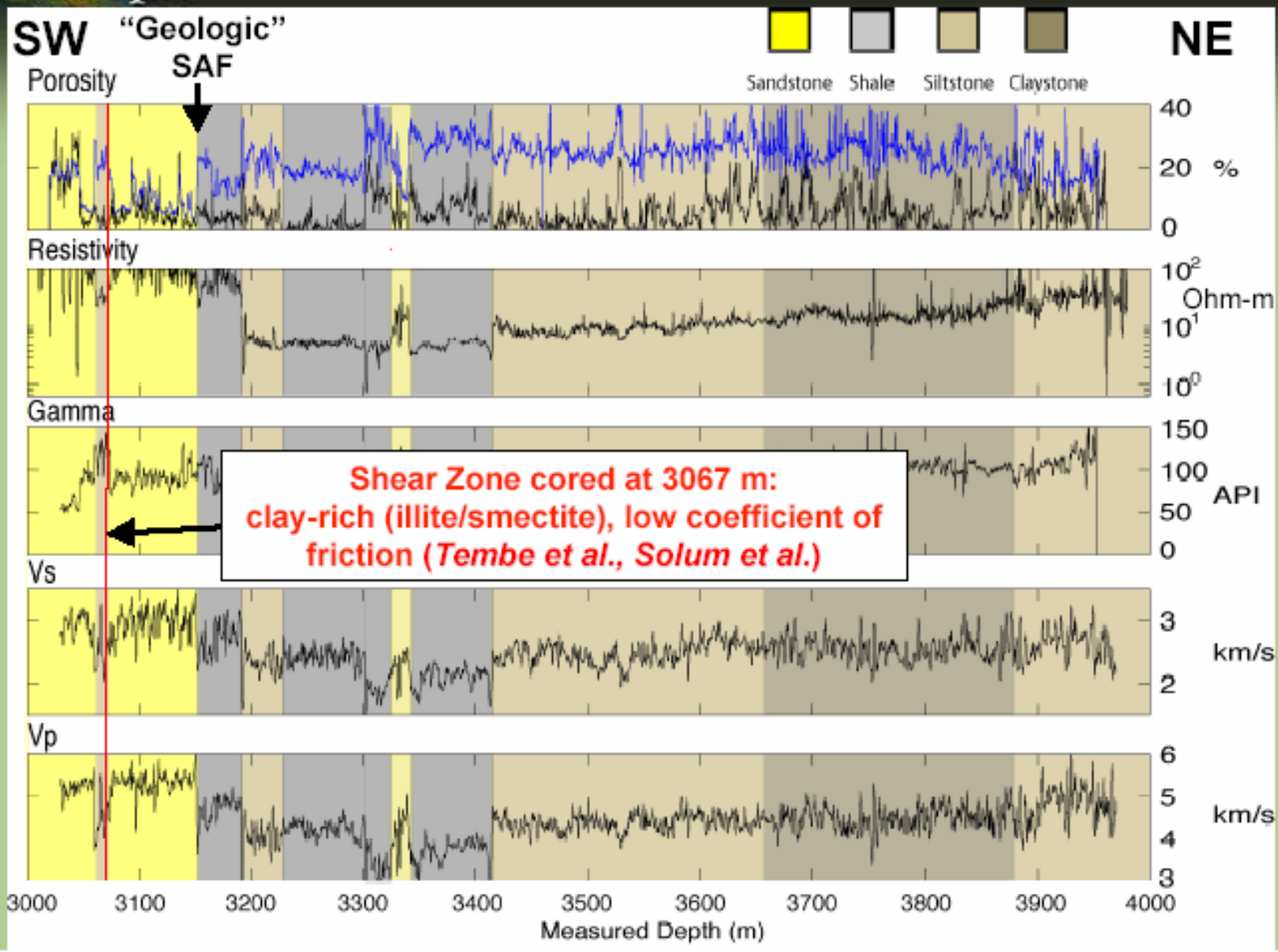

Shear Zone 3067 m MD

Weakest SAFOD samples

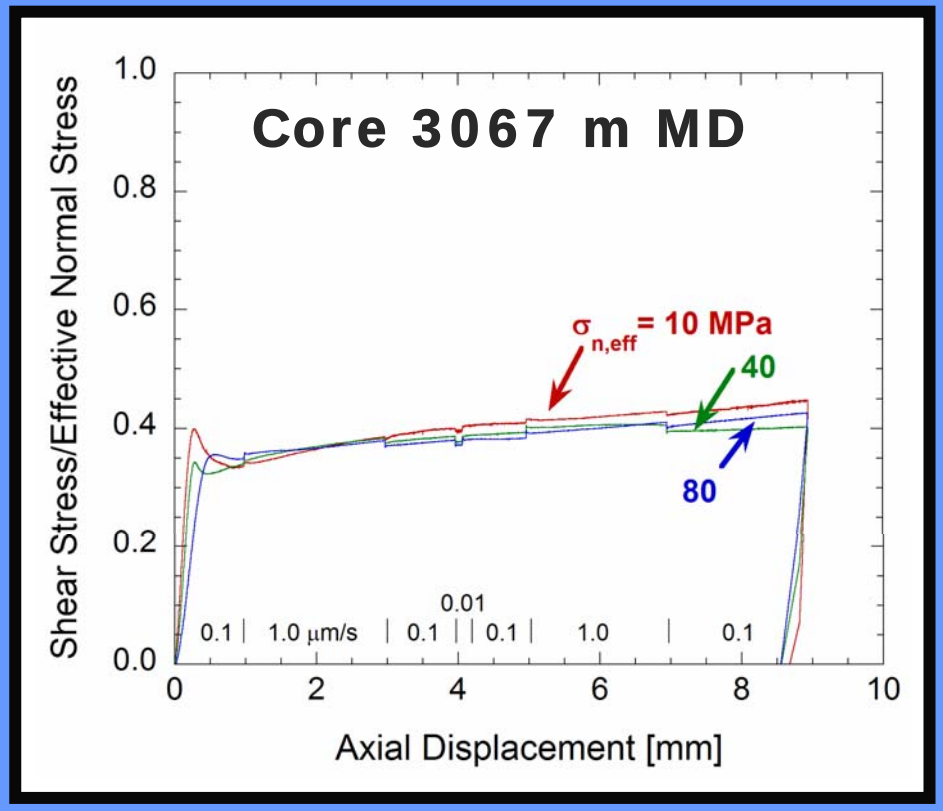

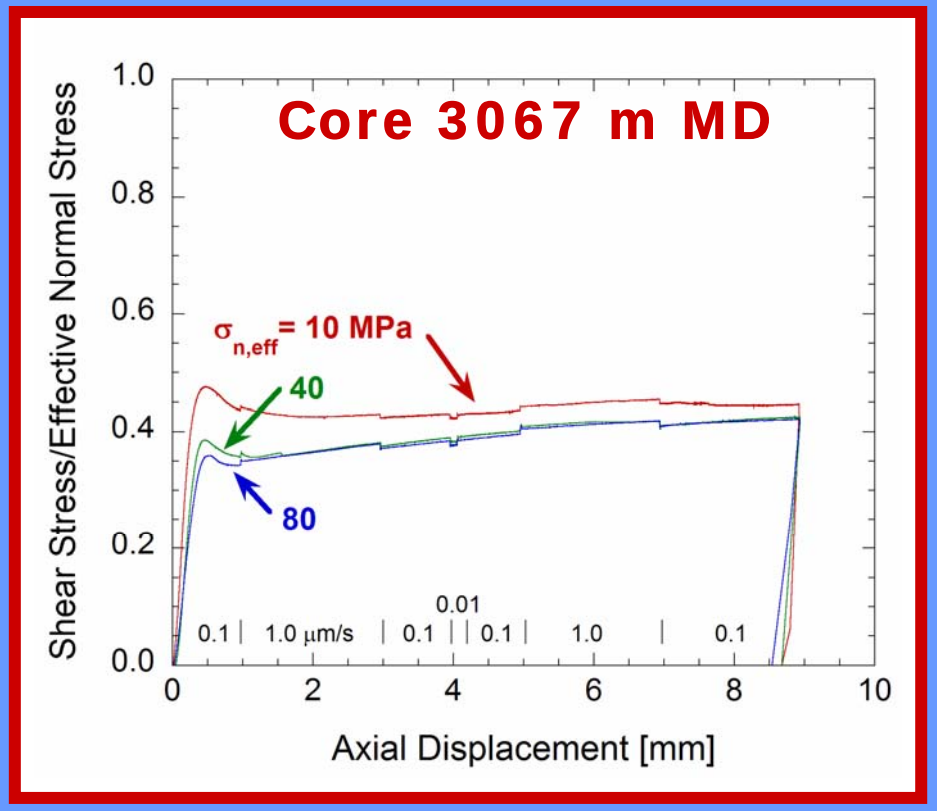

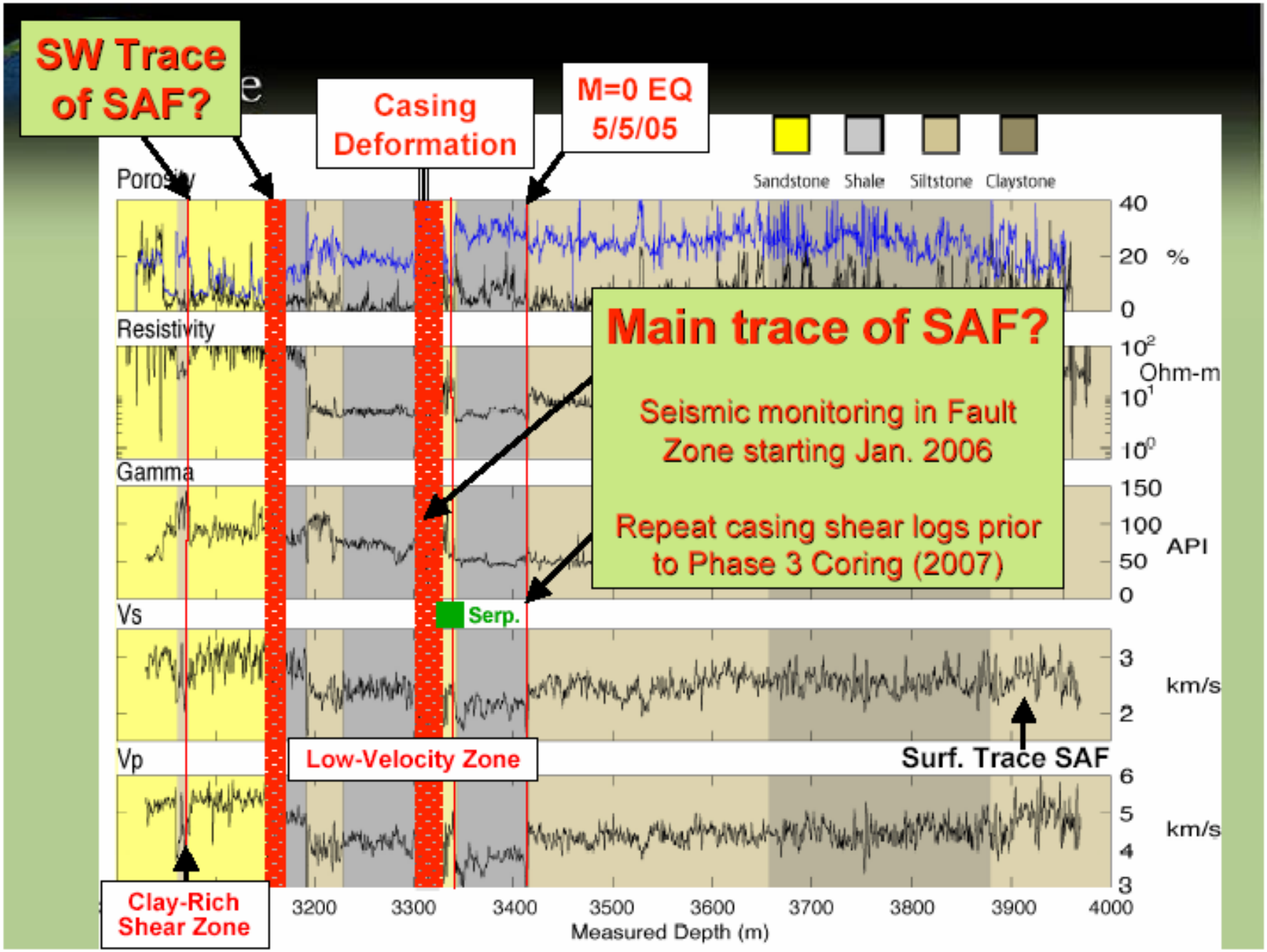
SW Trace of SAF?
Casing Deformation
M=0 EQ 5/5/05
Sandstone
Shale
Siltstone
Claystone
Porosity
40
20
%
0
Resistivity
10^2
Ohm-m
10^1
10^0
Gamma
150
100
API
50
0
Vs
Serp.
3
km/s
2
Vp
Low-Velocity Zone
Surf. Trace SAF
6
5
km/s
4
3
Clay-Rich Shear Zone
3200
3300
3400
3500
3600
3700
3800
3900
4000
Measured Depth (m)
Main trace of SAF?
Seismic monitoring in Fault Zone starting Jan. 2006
Repeat casing shear logs prior to Phase 3 Coring (2007)

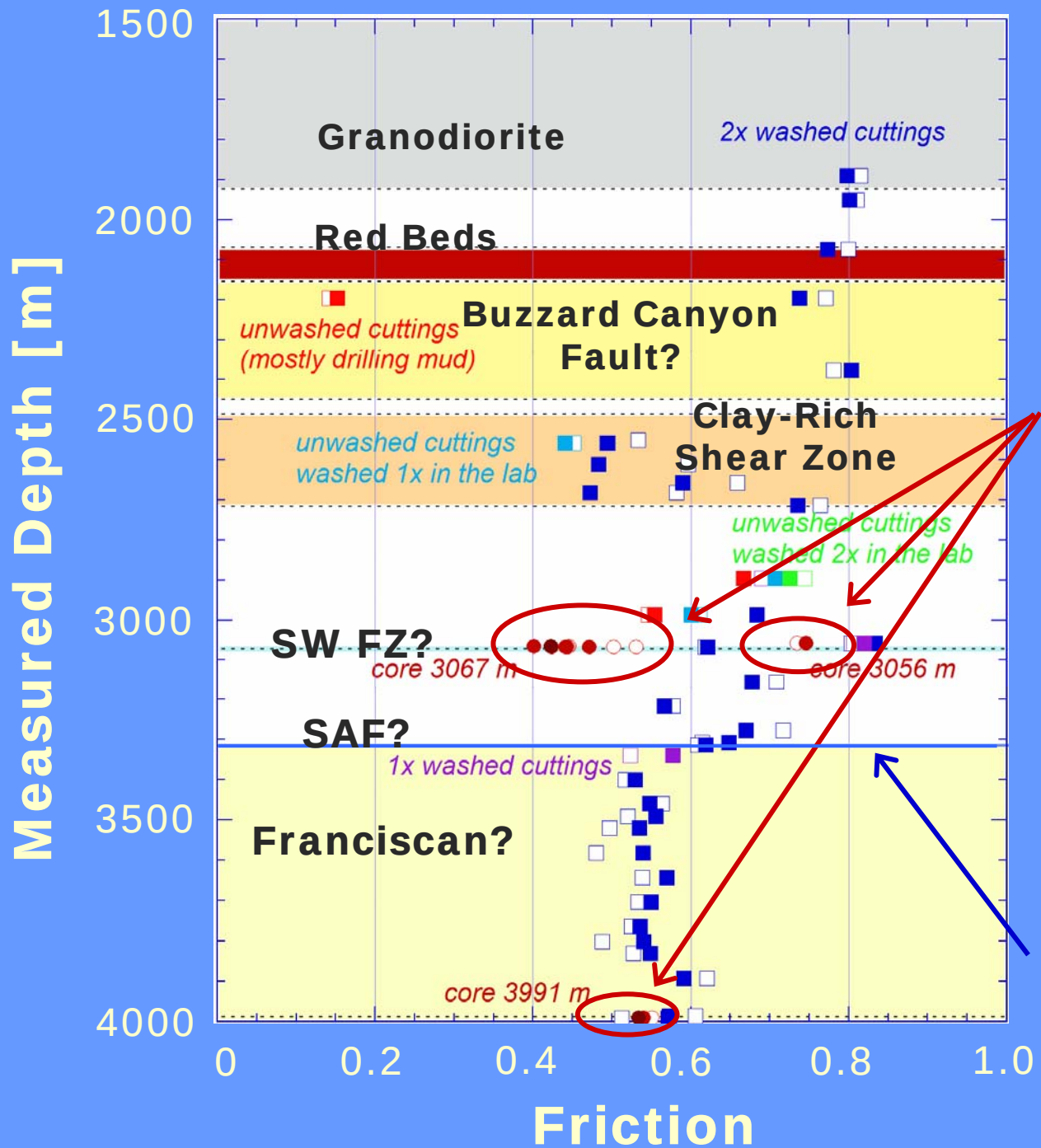

Squares: Cuttings
Circles: Core

Open symbols:
$\sigma_{n,eff}$ = 10 MPa

Solid Symbols:
$\sigma_{n,eff}$ = 40 MPa

Core

Saw-cut tests at 3056, 3066, 3067 and 3991 m ($\sigma_{n,eff}$=10, 40 and 80 MPa)

Strength tests on intact granodiorite core samples 1496 m (not shown here)

Active trace of the SAF?

Shear Zone 3067 m MD

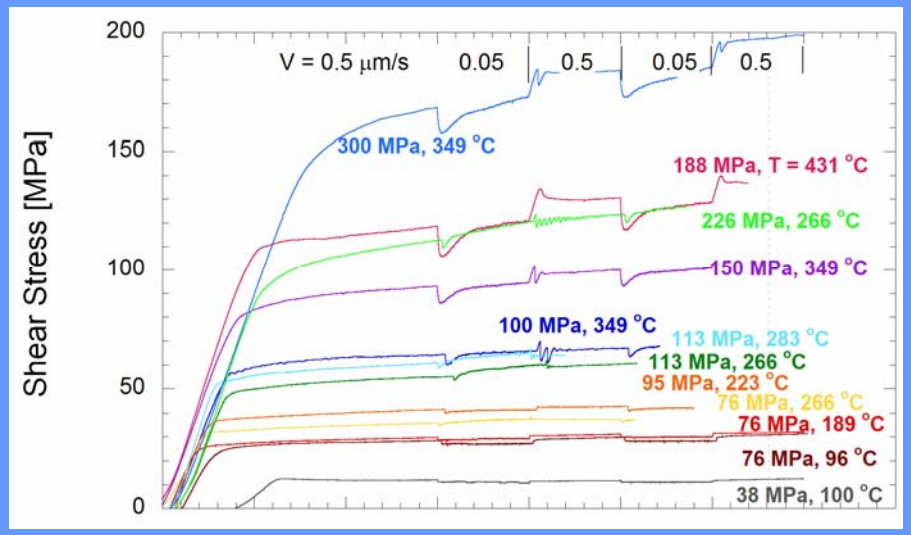

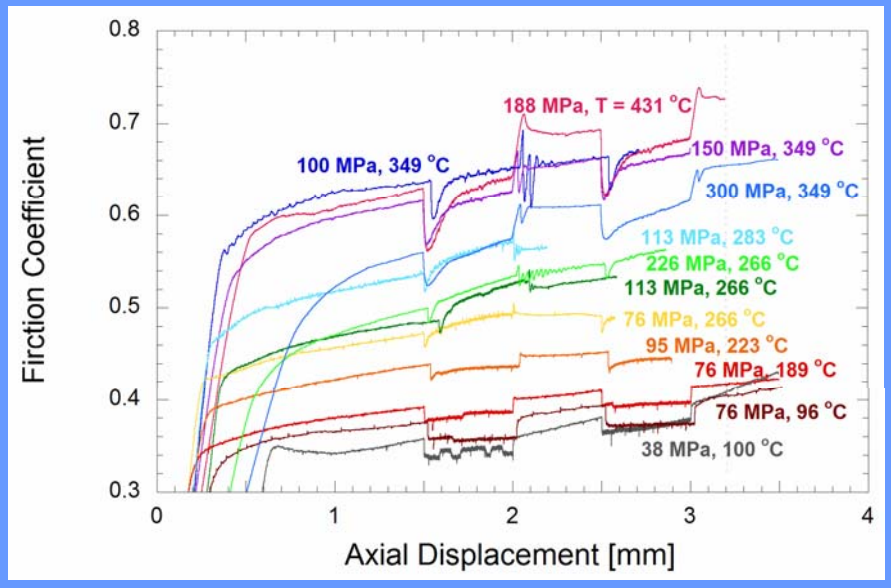

Frictional sliding tests on illitic fault gouge (SAFOD-MH-ST1 3067 m MD) at hydrothermal conditions under constant normal stress, pore pressure and temperature

(*Tembe et al.*, unpublished)

Hydrothermal experiments on fault gouge

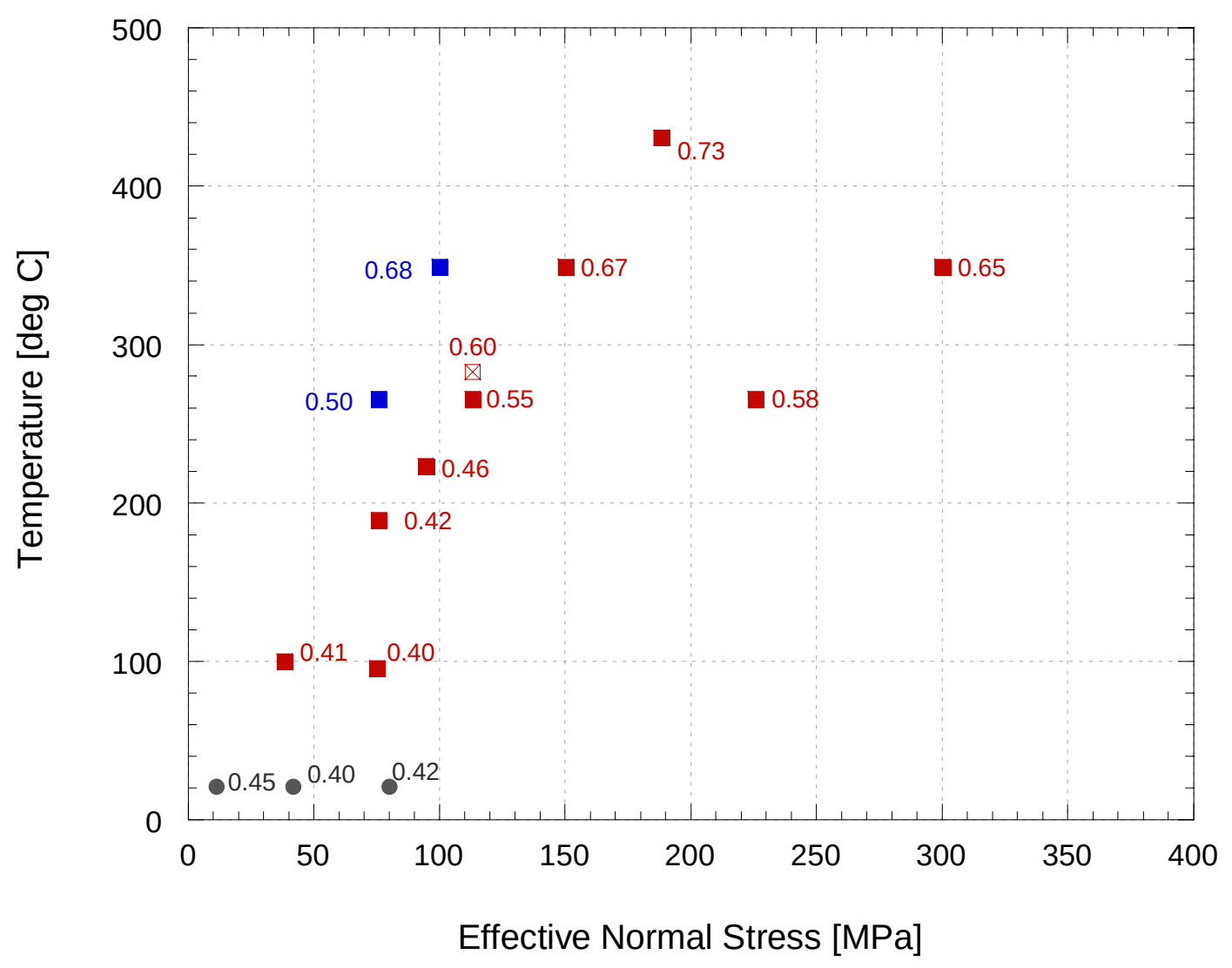

Key Points

- Best set of mechanical data to date with 59 experiments covering a depth range of 1890–3991 m
- Agreement between core and cuttings, XRD analysis and downhole logs
- Weakest samples tested have frictional strengths of $0.4 < \mu < 0.55$
  - elevated pore fluid pressure
  - dynamic weakening processes

Hydrothermal experiments on fault gouge

Constraints on pore pressure excess required for fault-normal compression

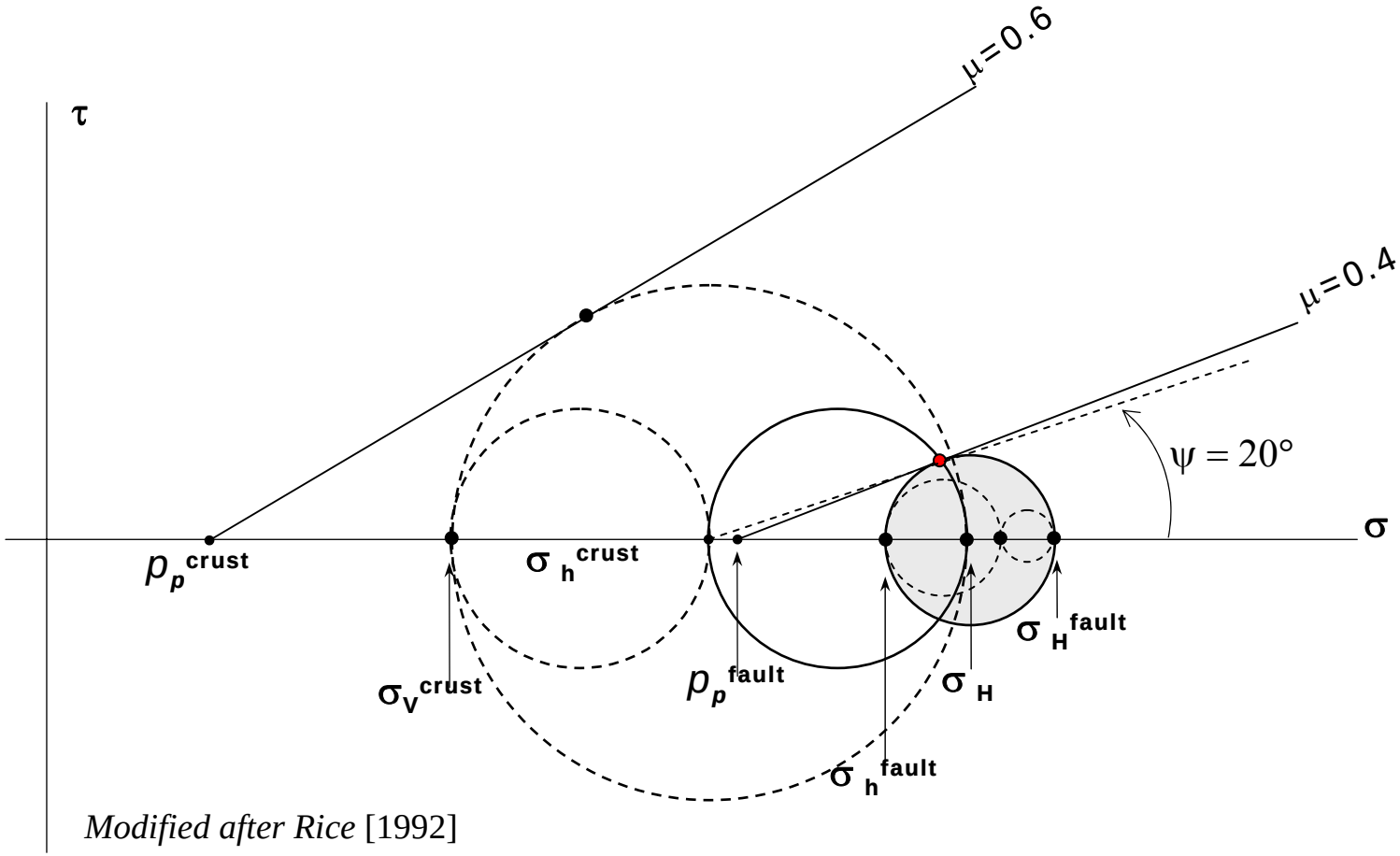

Modified after Rice [1992]

Phase 3 (summer 2007): Coring the Multi-Laterals

Lab Measurements on Continuous Core and Fluid Samples (***up to 1 km of core, recovered from creeping and seismogenic patches***):

- Mineralogy, elemental composition and isotope geochemistry: whole-rock, veins, and grain-scale.
- Deformation microstructures, particle and pore-size distribution,and textural analyses.
- Frictional strength and rheological properties (gouge and country rock).
- Physical properties (permeability, poroelastic, dilatational, seismic, thermal, resistivity, etc.).
- Liquid and gas geochemistry, bulk samples and fluid inclusions (major/minor elements and isotopes).
- Thermochronology and dating of host minerals and fault rock (U/Pb, Ar, FT annealing, ESR, TL dating).

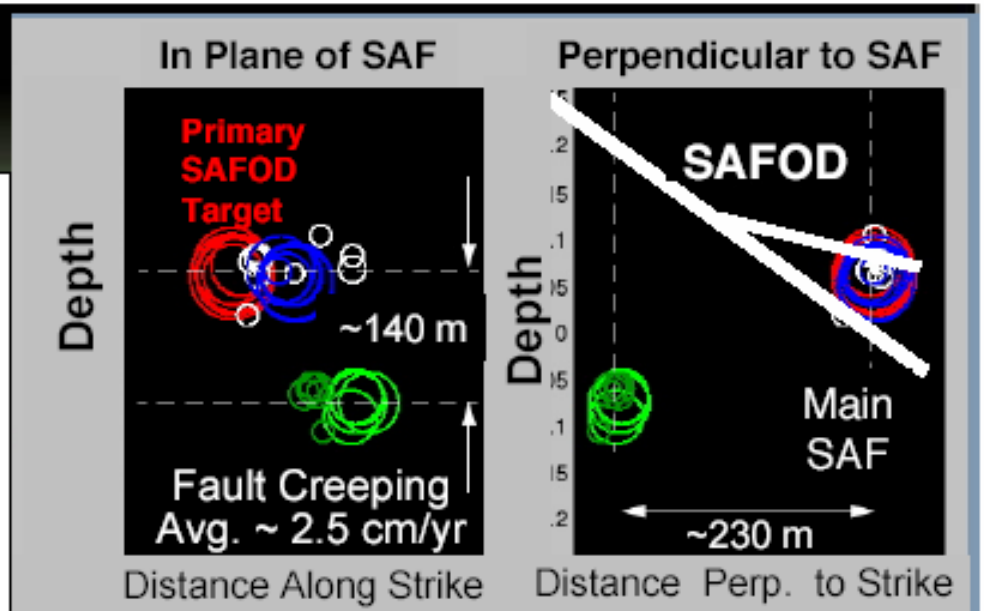

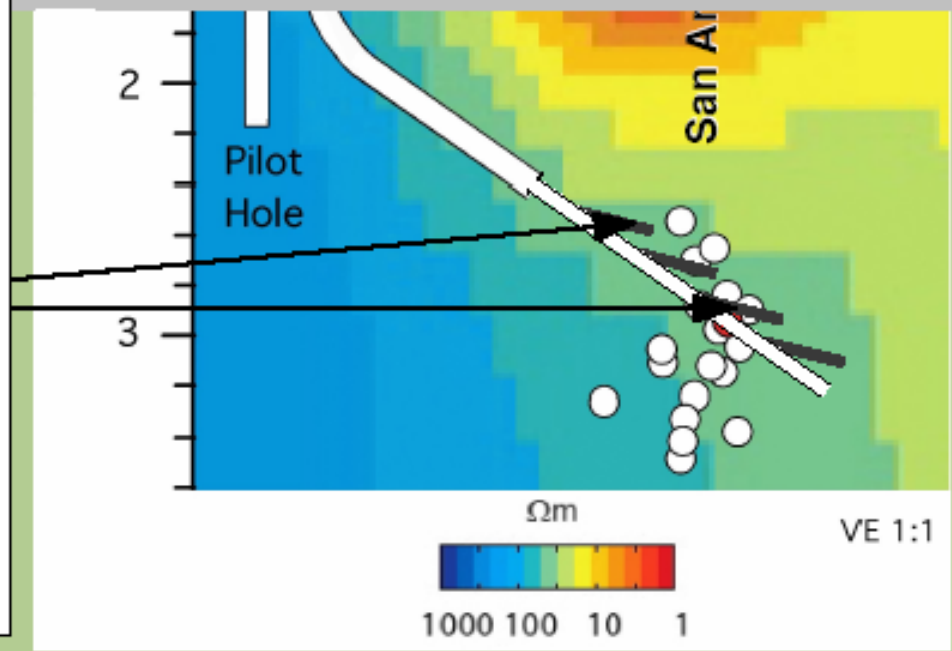

(*Hickman et al.*, AGU Fall Meeting 2005)

TCDP

Taiwan Chelungpu-fault Drilling Project

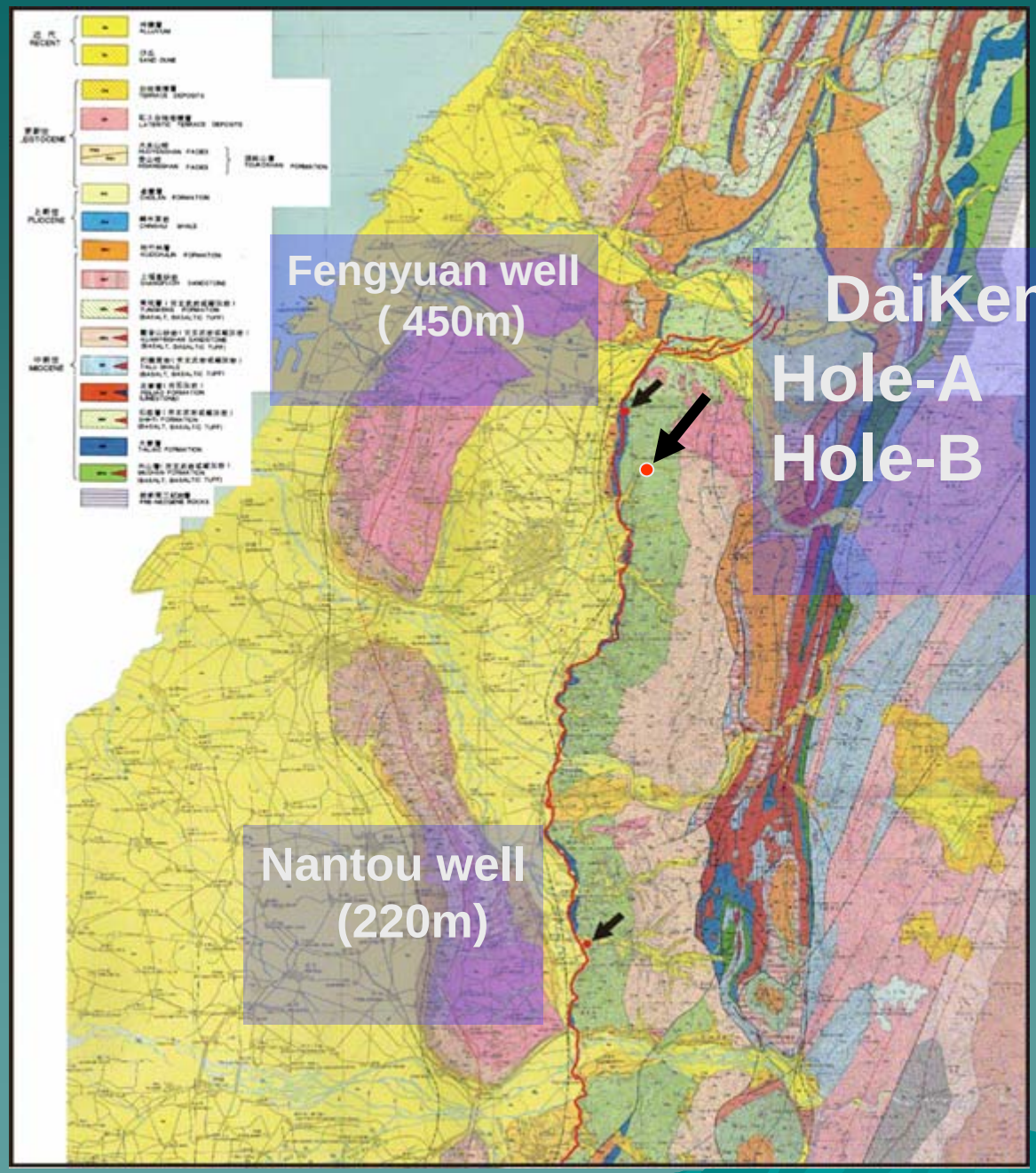
Fengyuan well
(450m)
DaiKeng well
Hole-A (2000m)
Hole-B (1350m)
Nantou well
(220m)

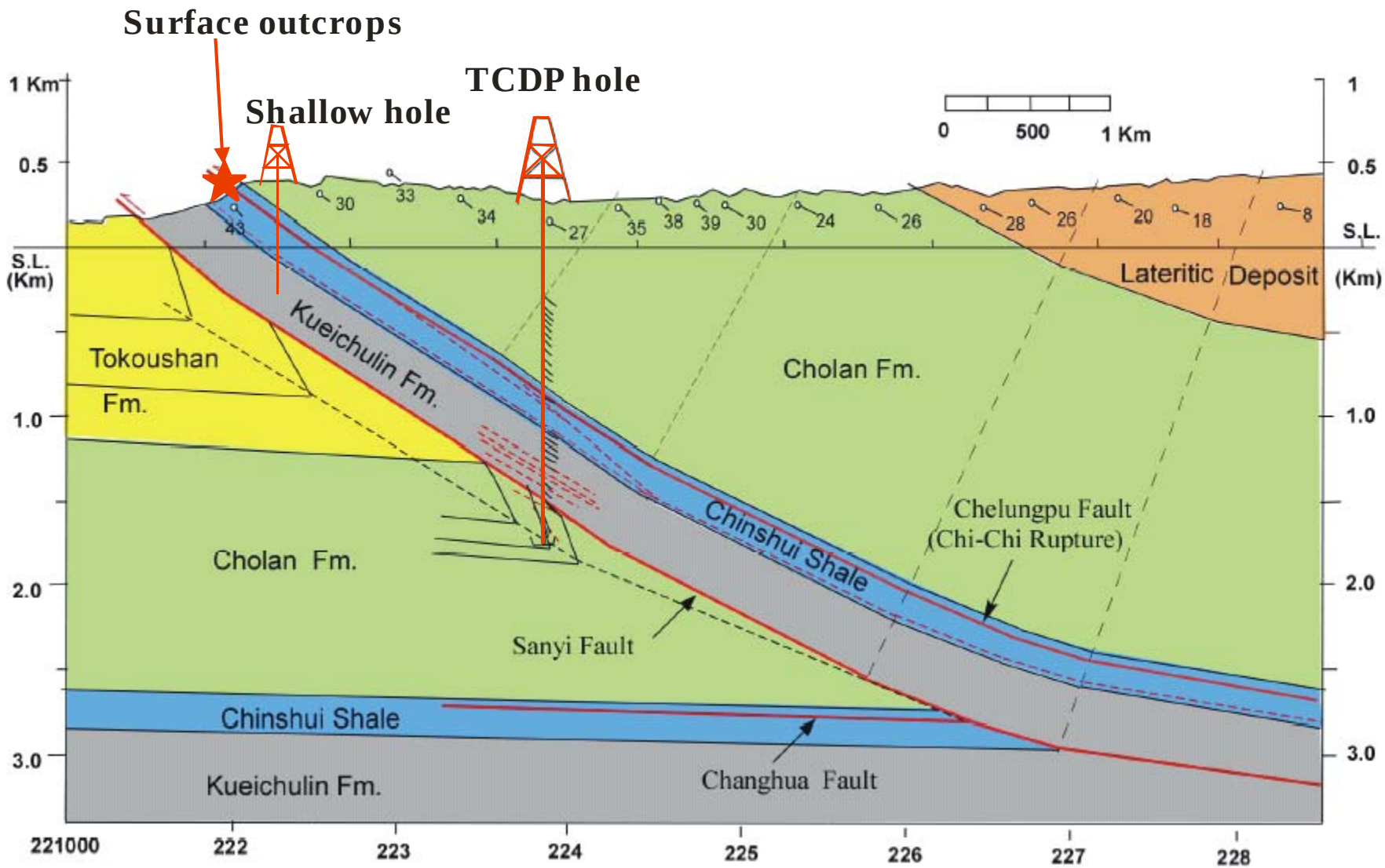
Surface outcrops
Shallow hole
TCDP hole
0
500
1 Km
1 Km
0.5
S.L.
(Km)
1.0
2.0
3.0
1
S.L.
(Km)
Lateritic Deposit
Tokoushan
Fm.
Kueichulin Fm.
Cholan Fm.
Cholan Fm.
Chinshui Shale
Chelungpu Fault
(Chi-Chi Rupture)
Sanyi Fault
Chinshui Shale
Kueichulin Fm.
Changhua Fault
221000
222
223
224
225
226
227
228

Fault zone FZ1111 (TCDP Hole A)

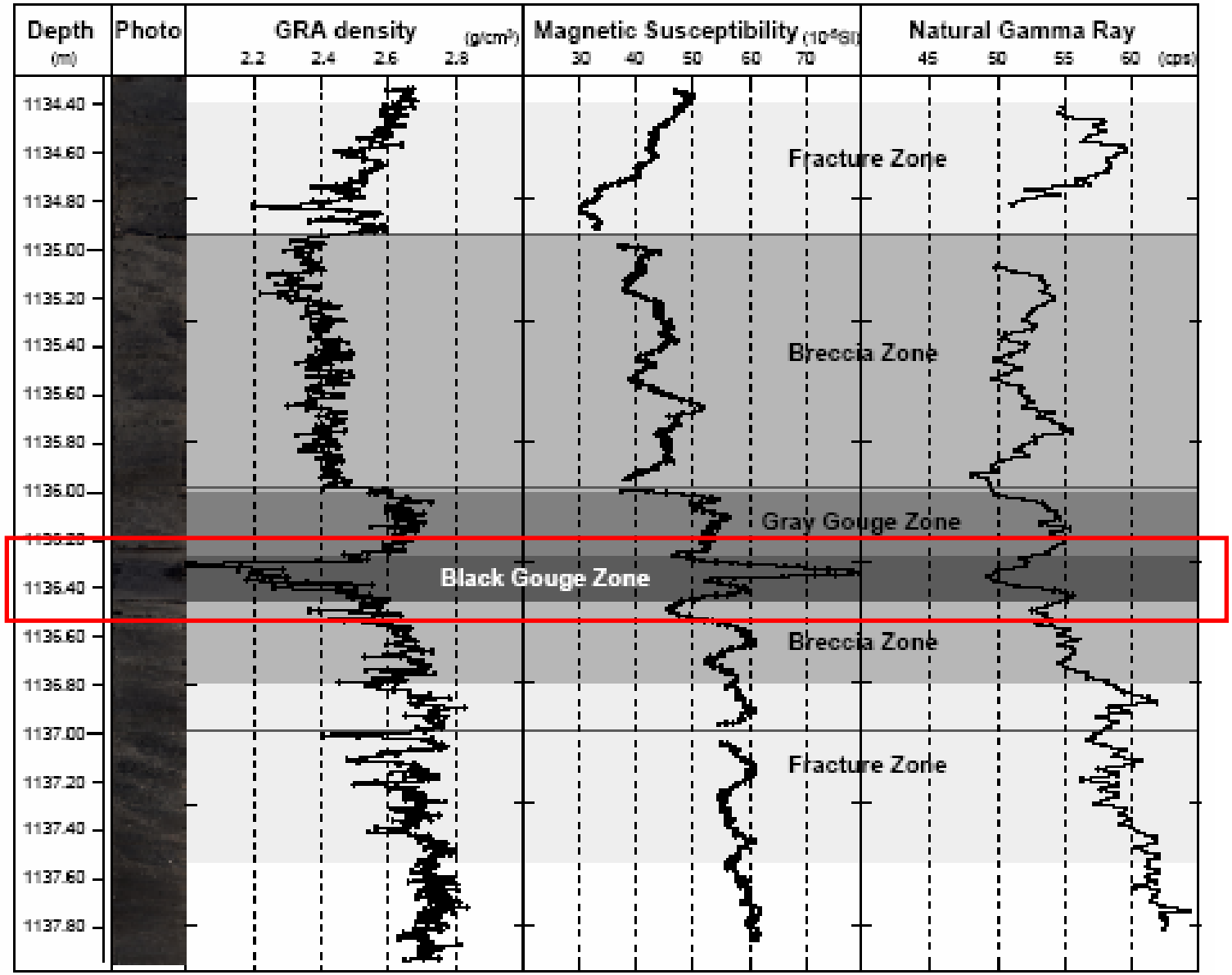

Hole-B Results

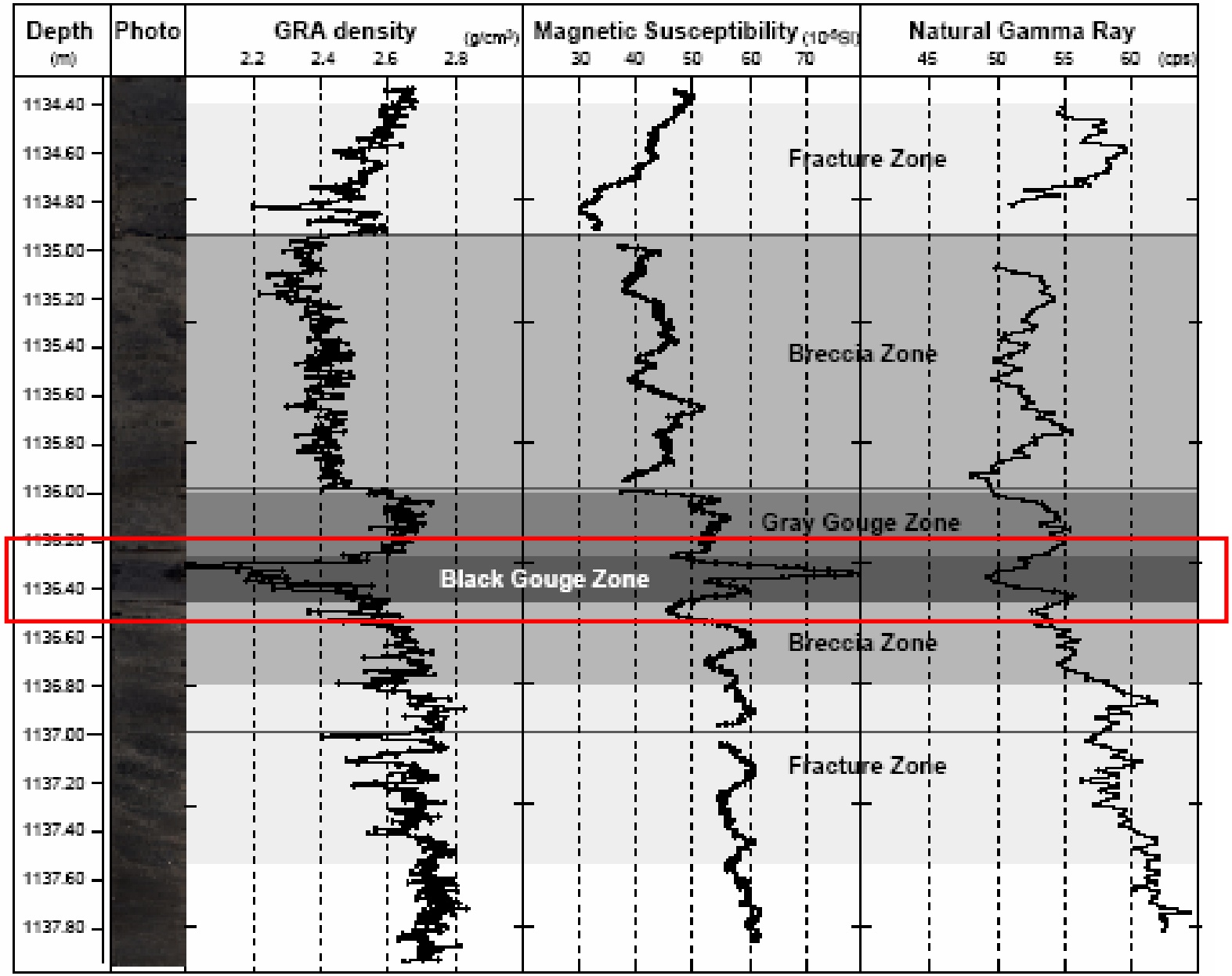

Anisotropy of *P*-wave velocity: 9 siltstone samples

Anisotropy of Magnetic Susceptibility: 9 siltstone and 6 sandstone samples

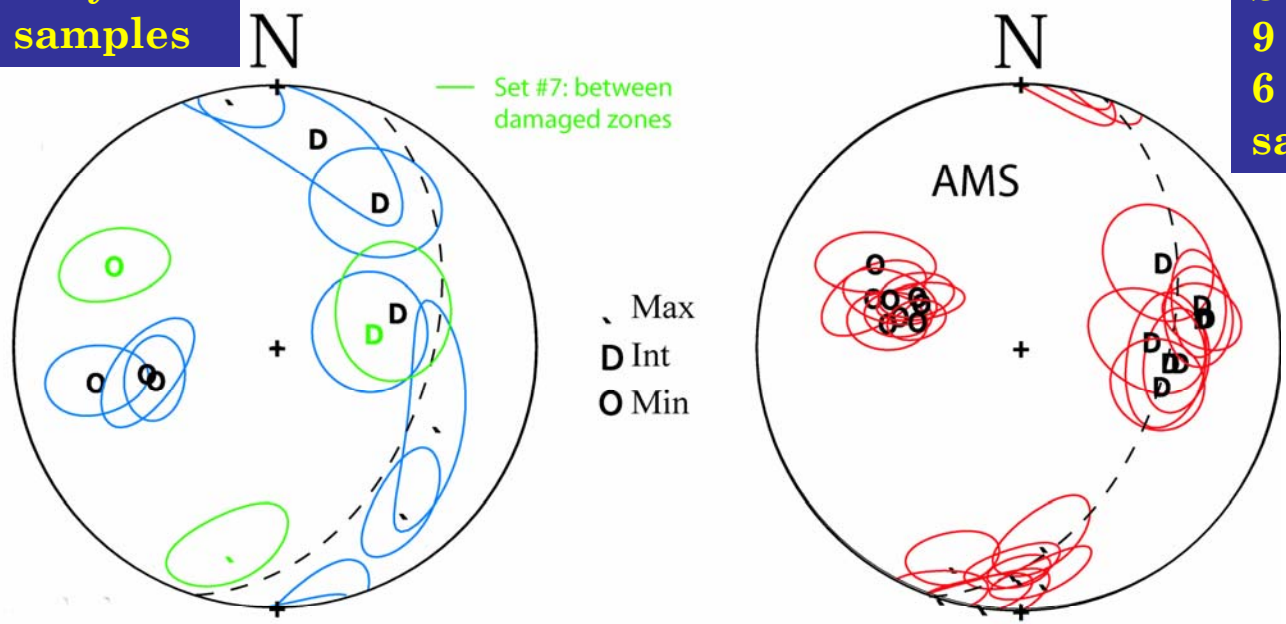

Silts:
$V_{P\ mean}$ = 3.45 km/s
Density = 2.6
Max anisotropy: 15%

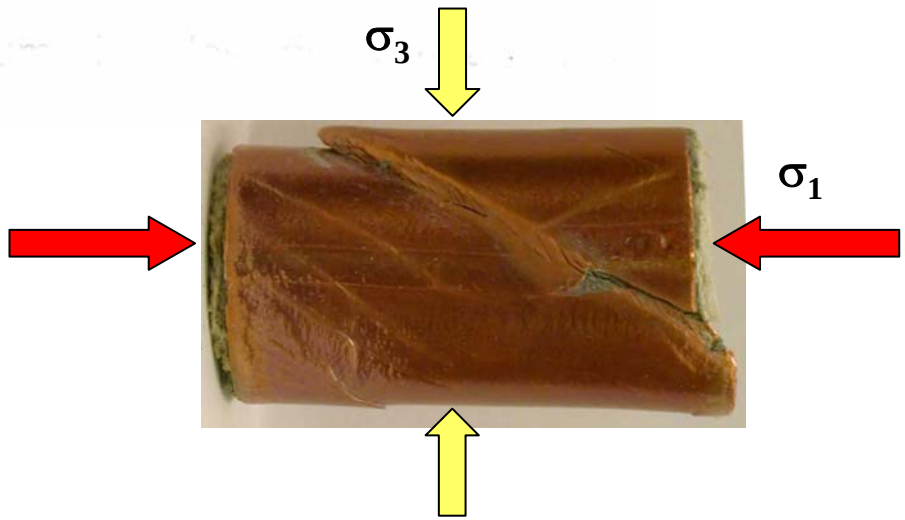

15 TCDP core samples from depths of 589-1368 m

(*Louis et al.*, 2006)

Taiwan TCDP Core - Gouge Friction

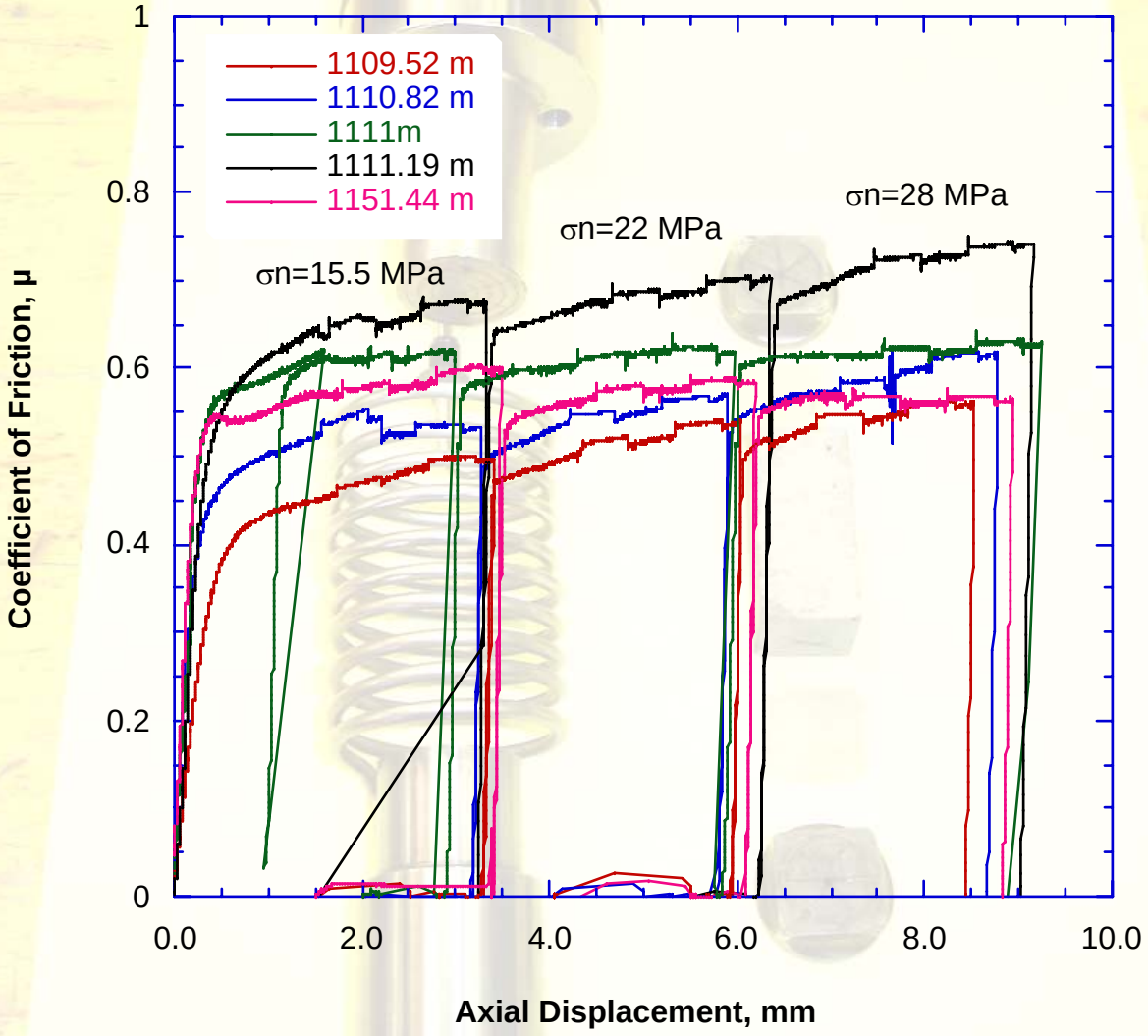

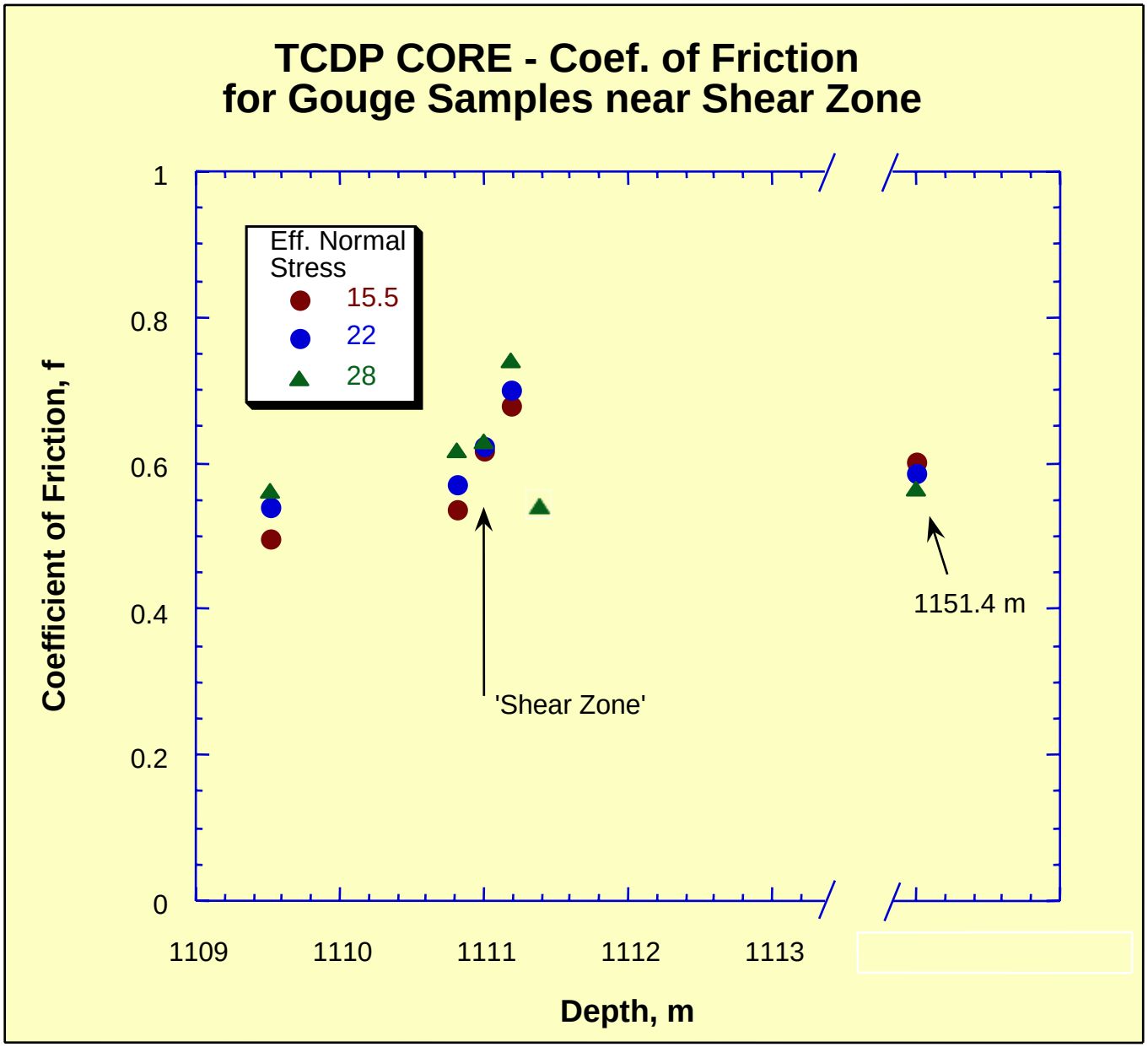
TCDP CORE - Coef. of Friction
for Gouge Samples near Shear Zone
Eff. Normal Stress
15.5
22
28
'Shear Zone'
1151.4 m
Coefficient of Friction, f
Depth, m
1
0.8
0.6
0.4
0.2
0
1109
1110
1111
1112
1113

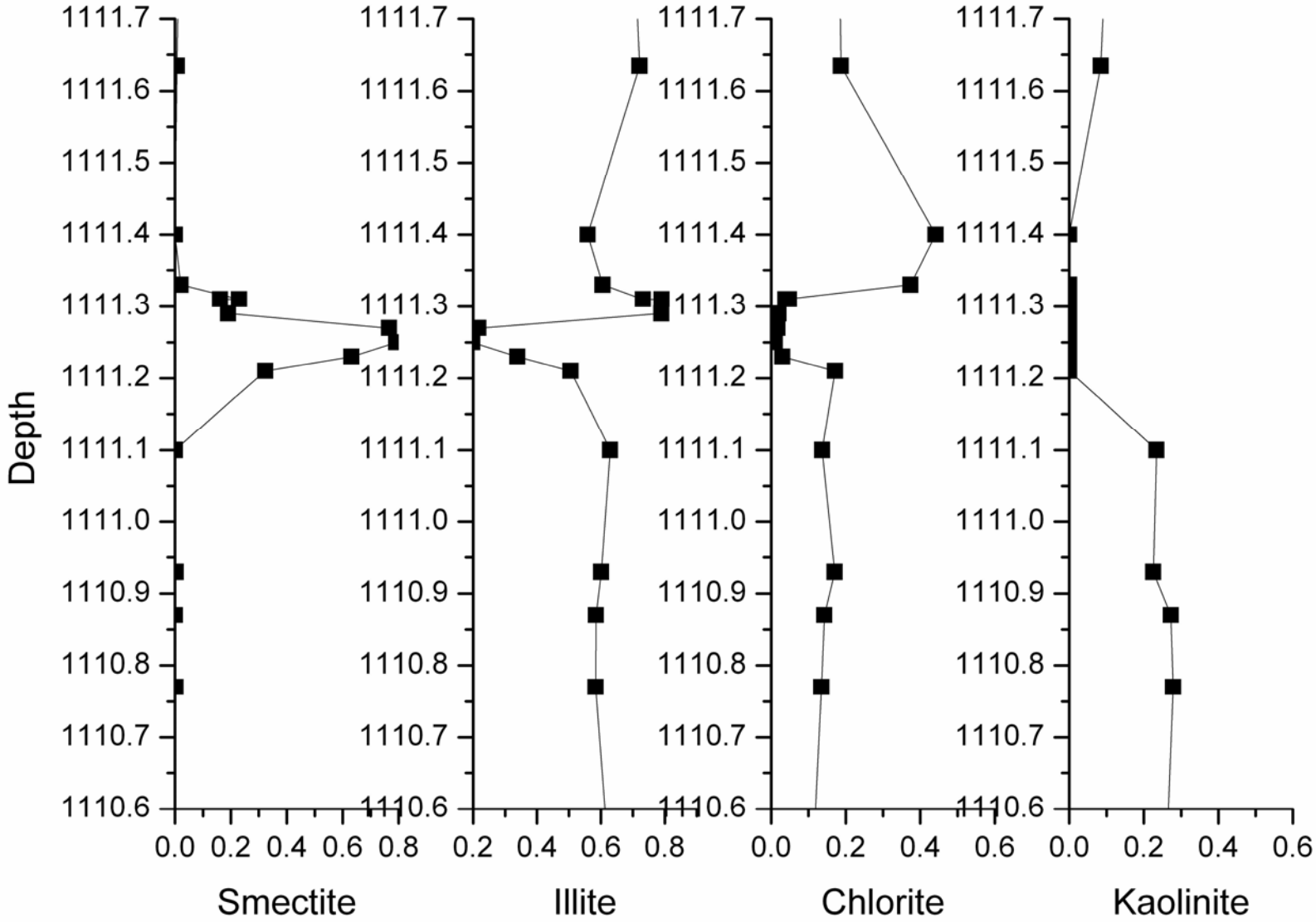

TCDP Hole A: Clay content (*Kuo & Song*., unpublished)

SAFOD Fault Rocks

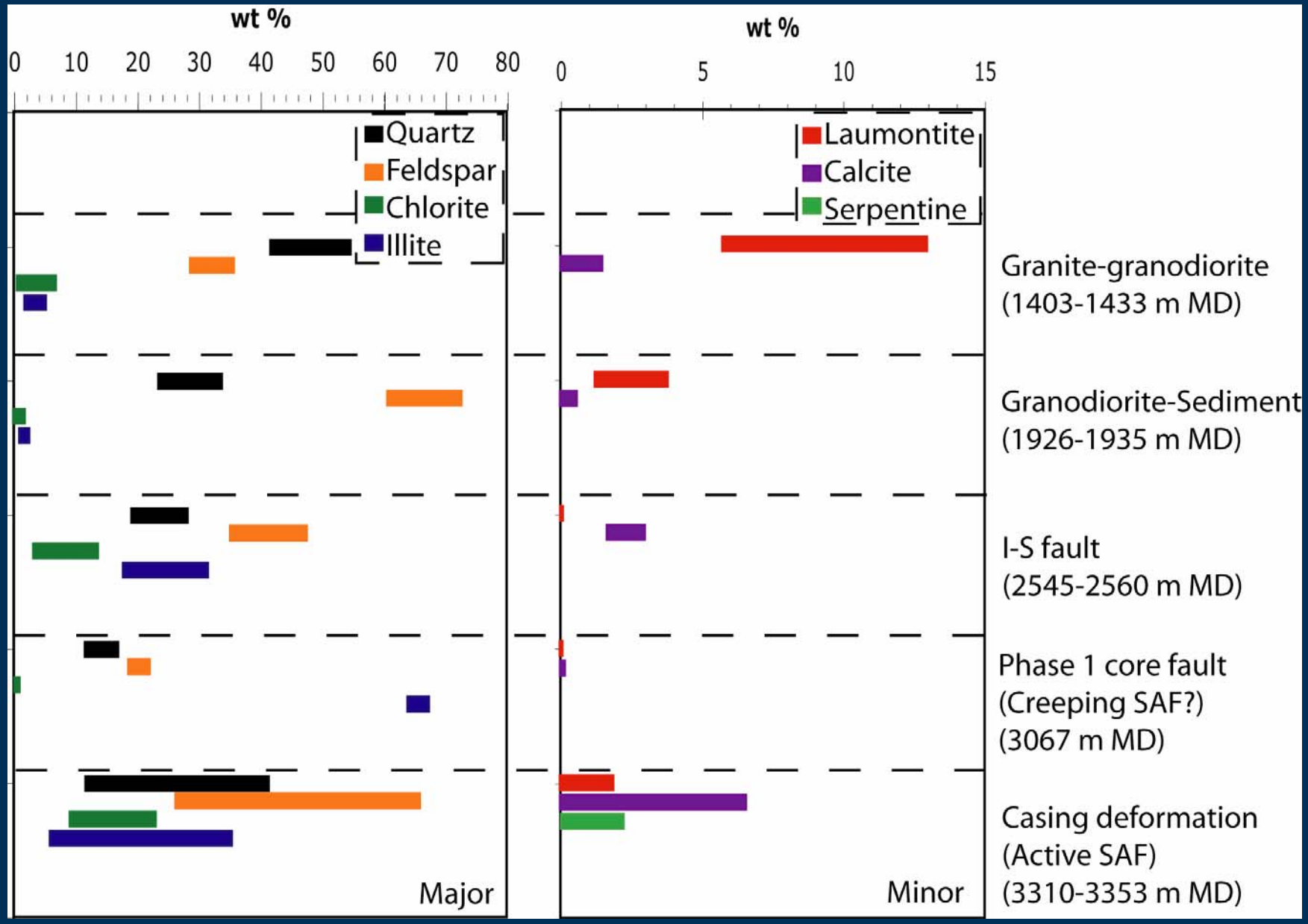

(*Solum et al.*, AGU Fall Meeting 2005)

Barbados Décollement microstructure (ODP Site 948)

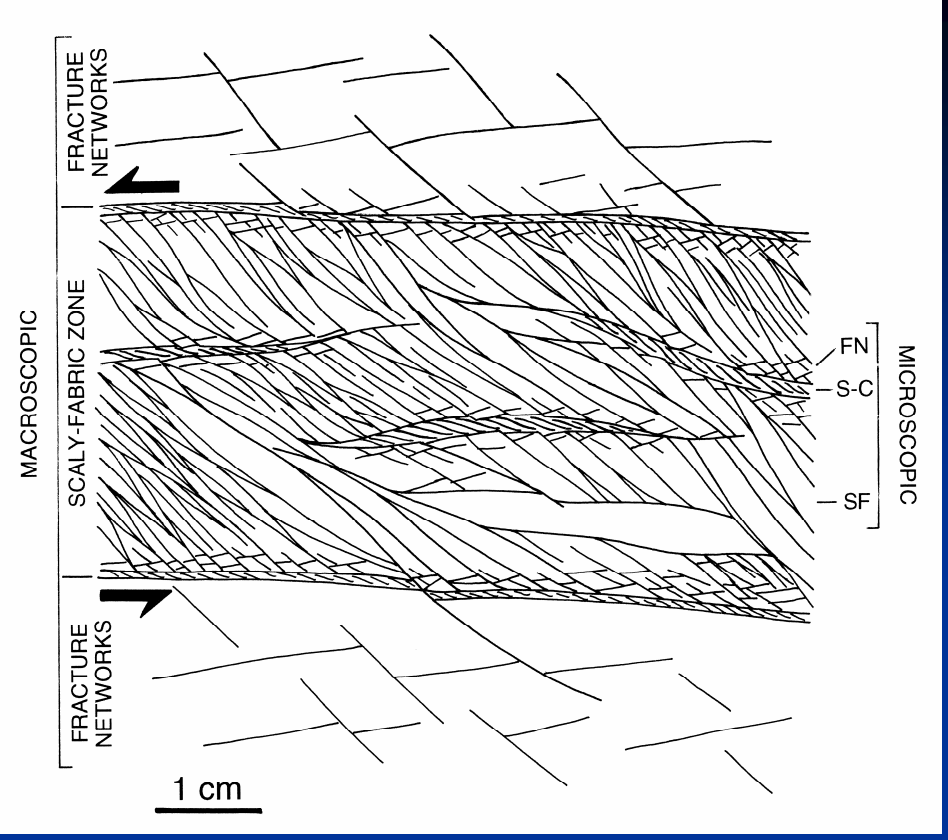

- Strongly foliated shear zones in brittlely fractured host
- An anomalously smectite clay-rich section
- S-C geometry in shear zones

Labaume et al., 1995

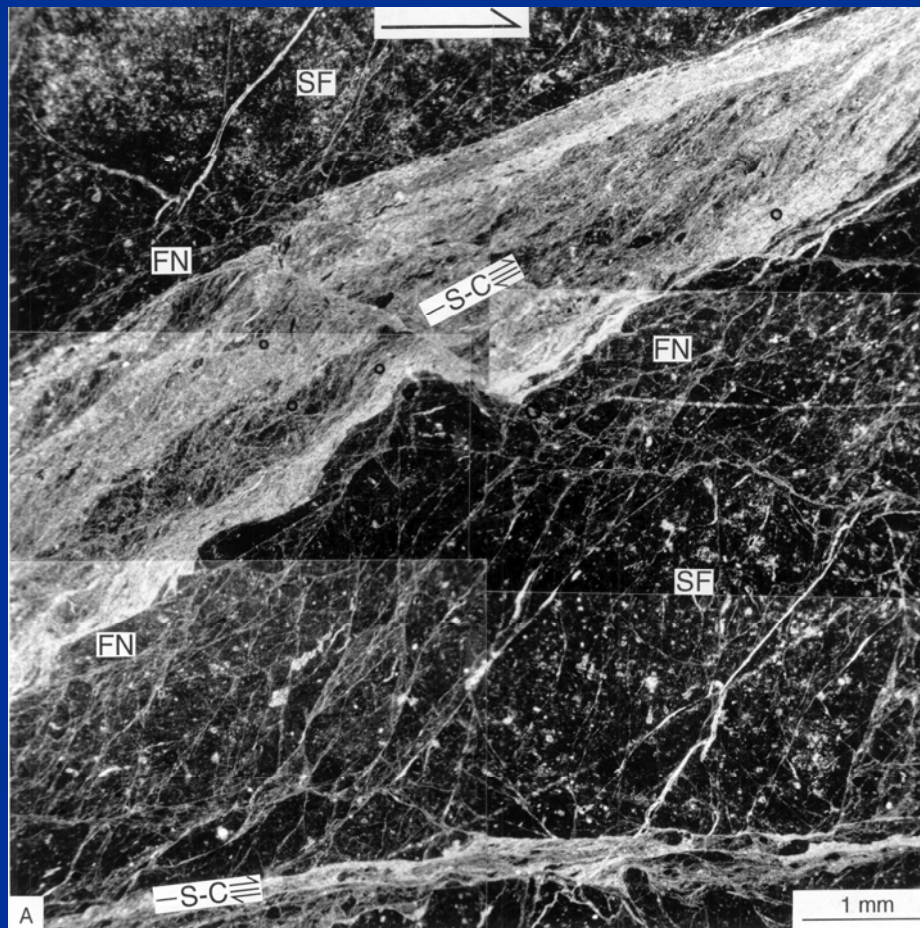

Fig. 61.
Frictional resistance of simulated gouge of crushed rock and minerals sheared between driving blocks of granite or sandstone (after Lockner and Beeler 2003a)

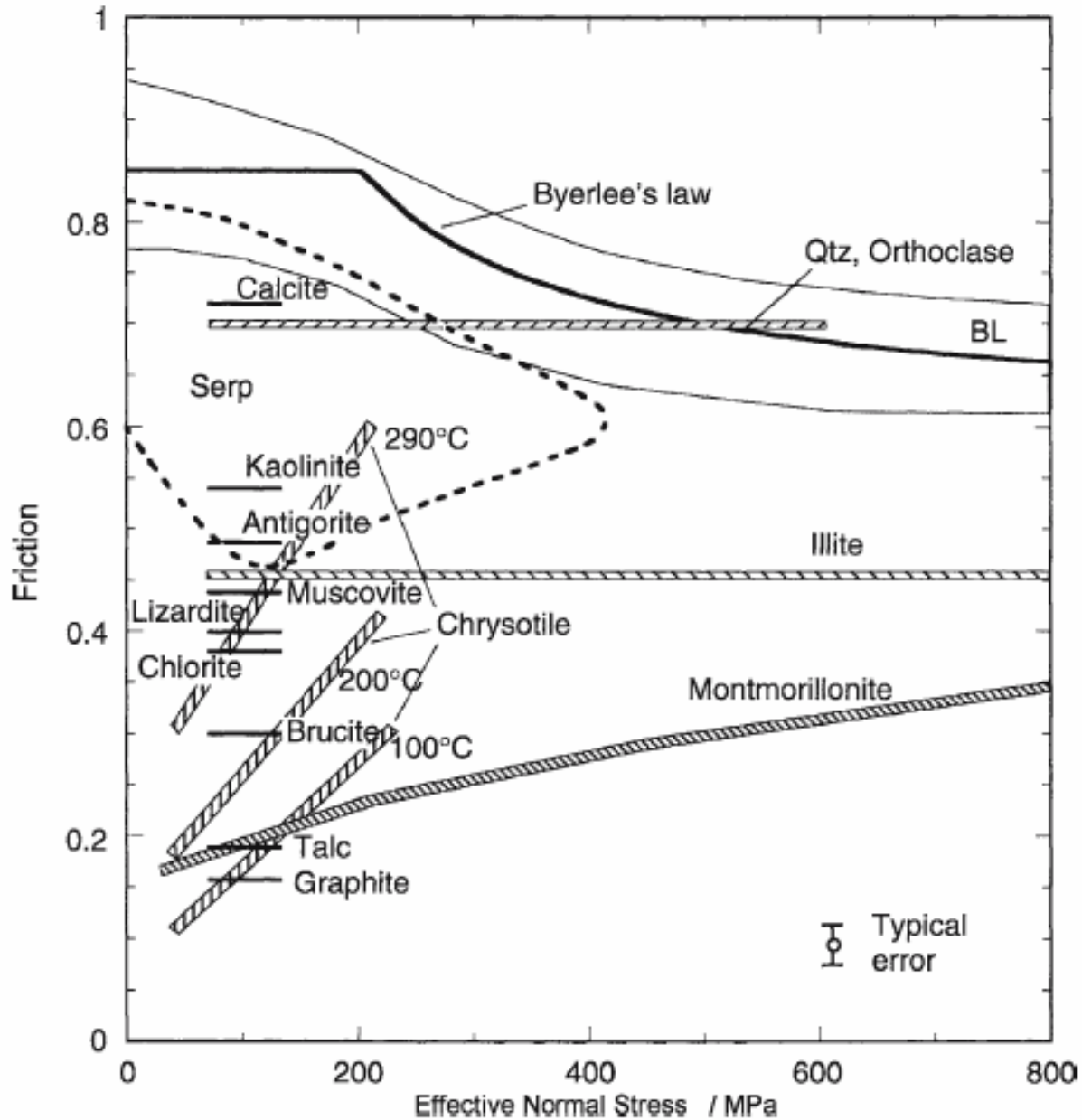

Coefficient of internal friction: Nankai mudstone Ring shear experiments

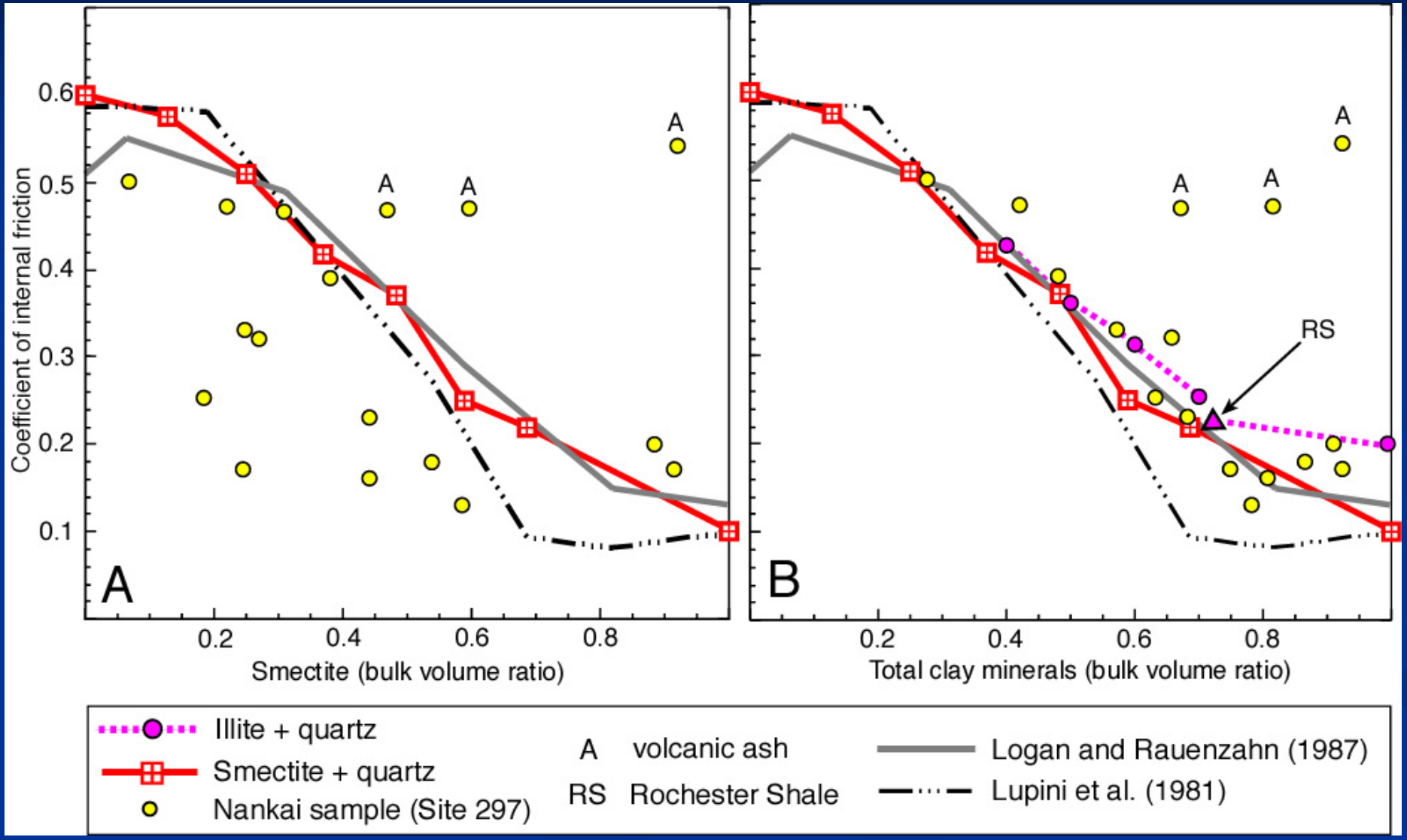

Brown et al. (2003)

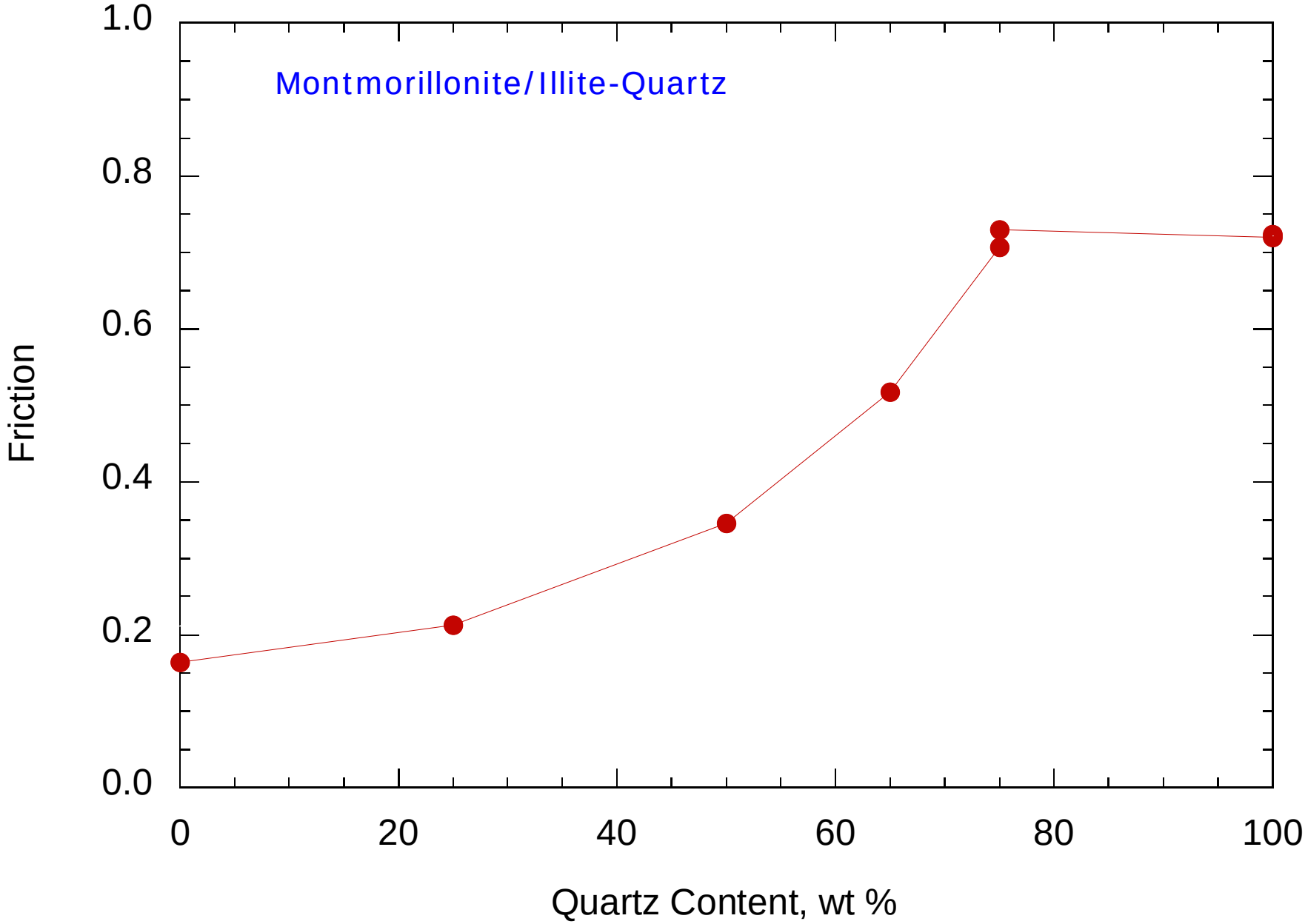

(*Tembe et al.*, unpublished)

Rate and State Dependence of Rock Friction

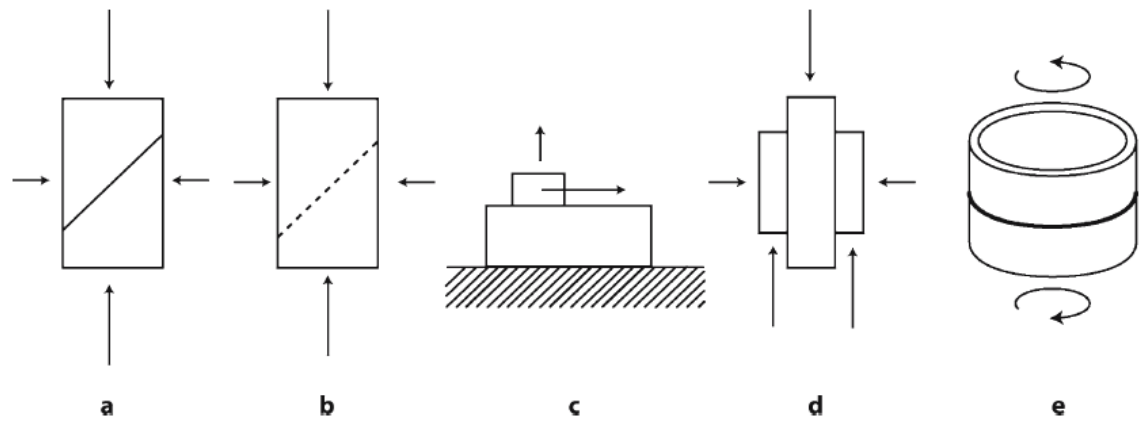

Fig. 58. Common types of friction tests. **a** Sliding on saw cut; **b** sliding on previously induced shear fracture; **c** conventional shear test; **d** double shear test; **e** rotary shear test

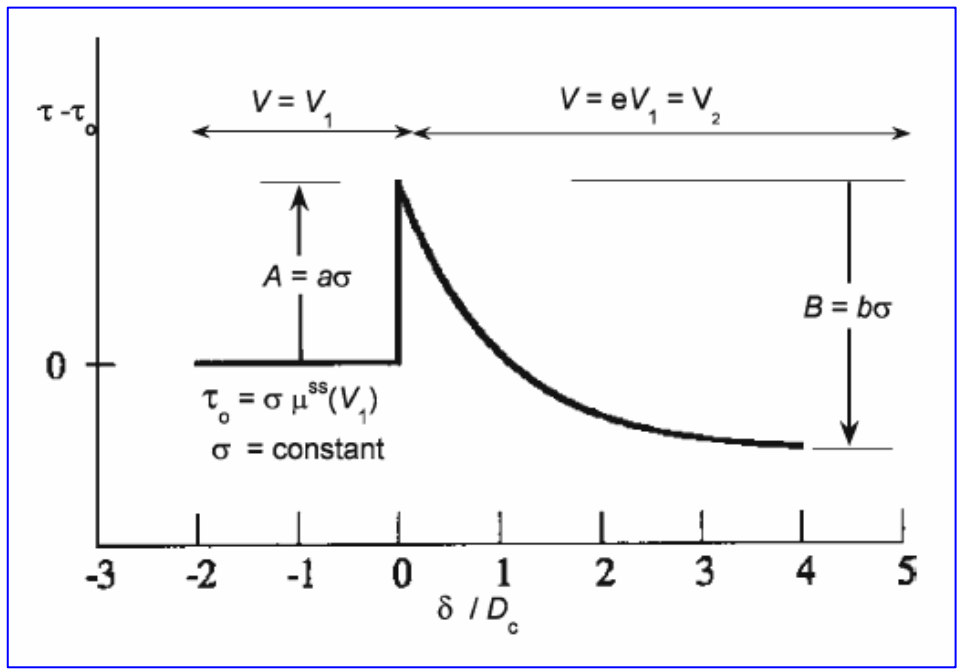

Fig. 63.
Velocity dependence of steady-state friction as a function of displacement, showing (**a**) a transition from initial velocity strengthening to steady velocity weakening for initially bare granite surfaces; (**b**) a similar transition for gouge layers but with more complicated subsequent behaviour (after Beeler et al. 1996)

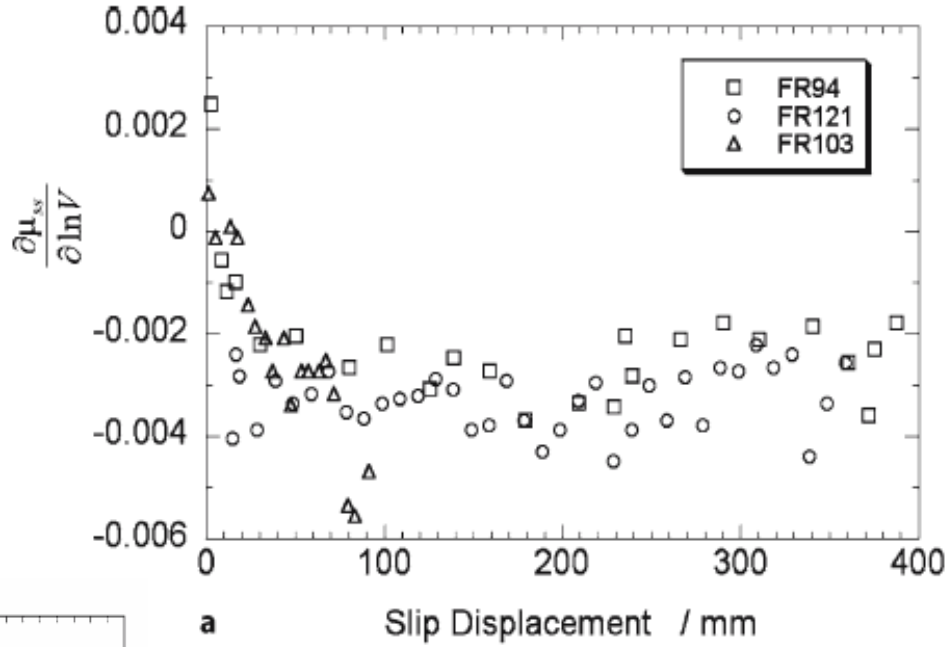

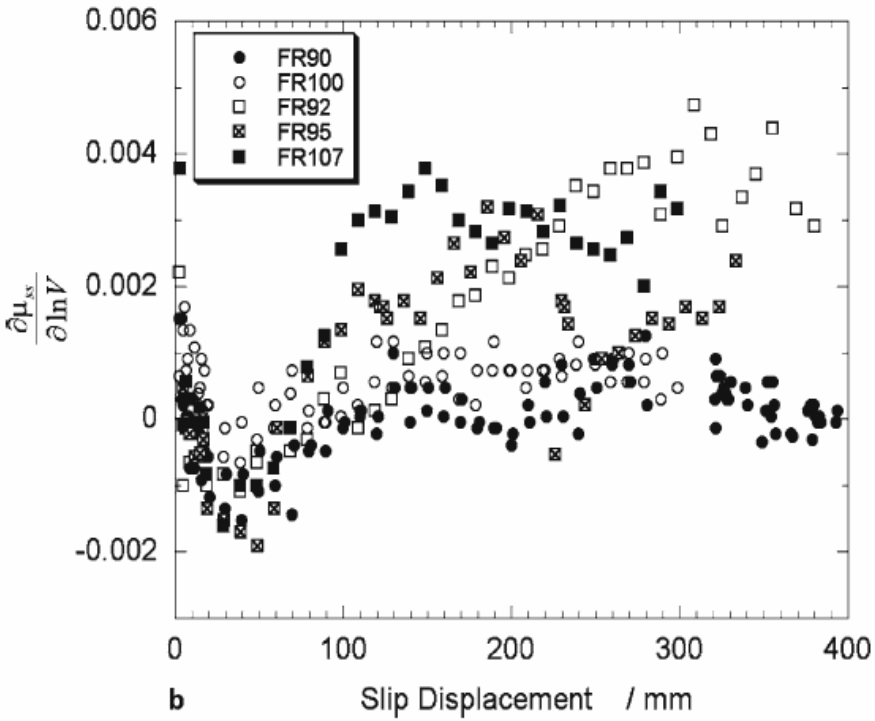

Table 7. Velocity dependence of the friction coefficient for steady state sliding at room temperature

Rock/gouge type	Normal stress (MPa)	Velocity dependence	Maximum $\left\lvert \frac{\partial \mu_{ss}}{\partial \ln V} \right\rvert$	Slip displacement (mm)	Sliding speed ($\mu m\ s^{-1}$)	Reference
Initially bare surface						
Granite	2	–	0.009	< 10	10^{-1}–10	Dieterich 1978, 1981
Granite	25	+	0.002	0 – 10	1–10	Beeler et al. 1996
	25	–	0.005	15 – 400	1–10	
Granite	5	–	0.003	6 – 24	10^{-3}–1	Kilgore, Blanpied and Dieterich 1993
	5	+	0.003	6 – 24	10–10^{3}	
	30 – 150	–	0.005	6 – 24	10^{-3}–10^{3}	
Granite	25	–	0.006	50 – 500	10^{-2}–10^{2}	Blanpied, Tullis and Weeks 1998
	25	+	0.009	50 – 500	10^{3}–3.2×10^{3}	
Granite (water saturated)	100	–	0.002	< 13	2×10^{-1}–10	Marone, Raleigh and Scholz 1990
Quartzite	3	–	0.009	< 10	0.01–2	Ruina 1980
Dolomite	75	+	0.005	2.5 – 4.7	10^{-2}–1	Weeks and Tullis 1985
Gabbro (smooth)	5	–	0.002	10 – 60	10^{-1}–10	Marone and Cox 1994
Gabbro (rough)	5	–	0.006	2 – 38	10^{-1}–10	
	5	+	0.001	54 – 62	10^{-1}–10	
Serpentinite (antigorite)	25 – 125	+	0.018	< 400	3.2×10^{-3}–3.2×10^{2}	Reinen et al. 1991
	25 – 125	–	0.005	< 400	10^{-1}–10	

Velocity dependence of steady-state friction: **initially bare** rock surfaces (*Paterson & Wong*., 2005)

Table 7. *Contiuned*

Rock/gouge type	Normal stress (MPa)	Velocity dependence	Maximum $\left\lvert \frac{\partial \mu_{ss}}{\partial \ln V} \right\rvert$	Slip displacement (mm)	Sliding speed ($\mu m\ s^{-1}$)	Reference
Simulated gouge layer						
Crushed granite	10	+	0.004	< 2.5	2.5×10^{-1}–25	Dieterich 1981
	10	–	0.005	2.5 – 8	2.5×10^{-1}–25	
Crushed granite	25	–	0.002	20 – 60	1–10	Beeler et al. 1996
	25	+	0.004	100 – 400	1–10	
Crushed granite	50 – 600	+	0.007	< 10	7×10^{-3}–7	Solberg and Byerlee 1984
Feldspar	25	–	0.008	30 – 170	10^{-3}–10	Scruggs and Tullis 1998
Quartz	25 – 70	+	0.014	2 – 4	10^{-3}–10	Mair and Marone 1999
	25 – 70	–	0.007	8 – 16	10^{-3}–10	
Quartz (water saturated)	50 – 190	+	0.004	< 13	10^{-1}–30	Marone, Raleigh and Scholz 1990
Illite, montmorillonite, and mixture (saturated)	360 – 400	+	0.007	< 8	10^{-2}–1	Morrow, Radney and Byerlee 1992
Quartz–montmorillonite mixture (saturated)	55 – 81	+	0.008	< 12	3×10^{-3}–2×10^{2}	Logan and Rauenzahn 1987
Muscovite	25 – 150	+	0.006	< 200	10^{-3}–10	Scruggs and Tullis 1998
Biotite	25	–	0.006	< 150	10^{-3}–10	Scruggs and Tullis 1998
Serpentinite (antigorite, chrysotile)	25 25	+ –	0.04 0.01	< 276 < 276	10^{-3}–10^{-1} 1–32	Reinen, Weeks and Tullis 1994

Velocity dependence of steady-state friction: **simulated gouge layers**

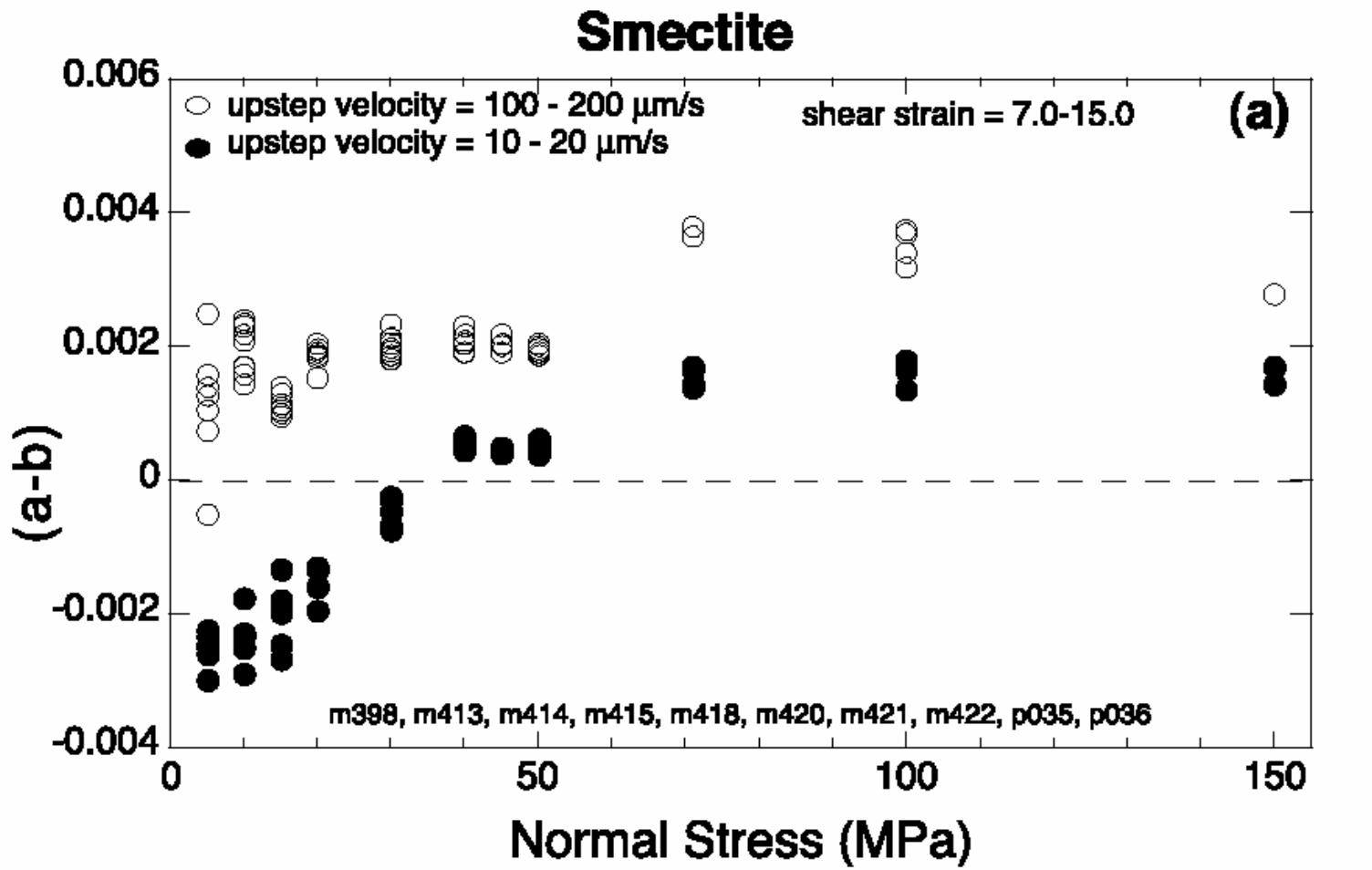

velocity dependence behavior of unsaturated clay gouge (*Saffer & Marone*, 2003)

Permeability of Core Samples from Fault Zones

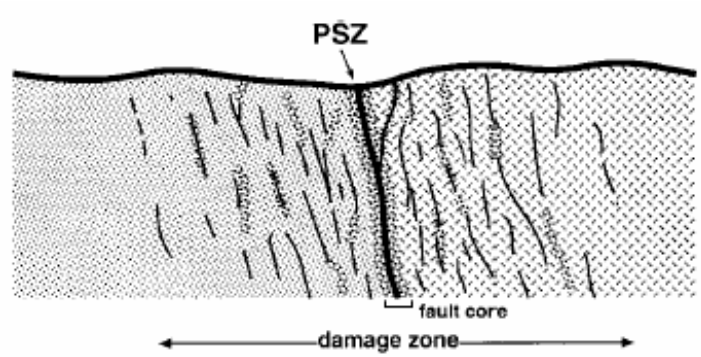

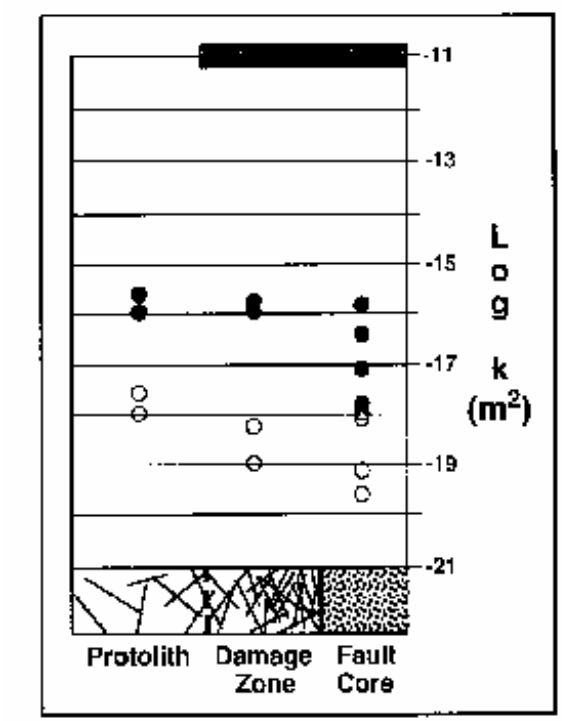

Dixie Valley (*Seront et al.*, 1998)

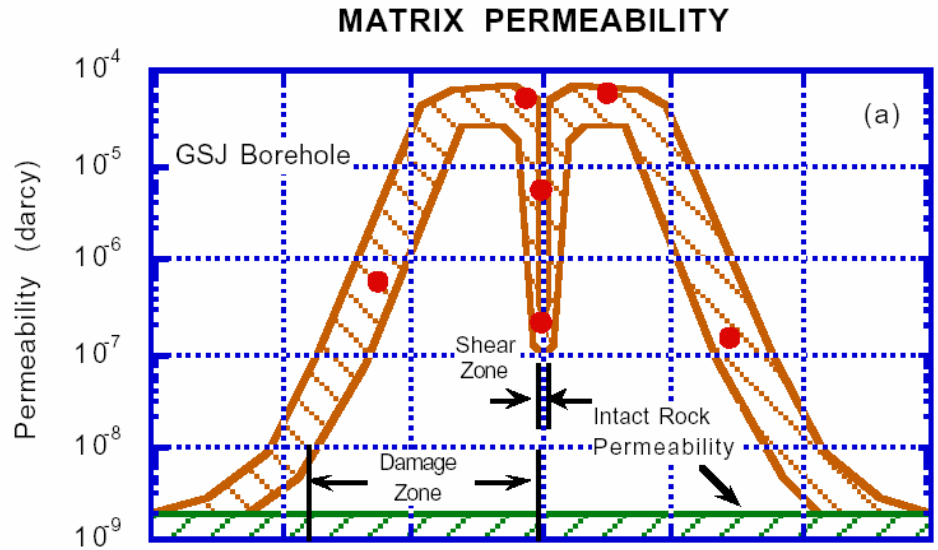

Nojima fault (*Lockner et al.*, 1999)

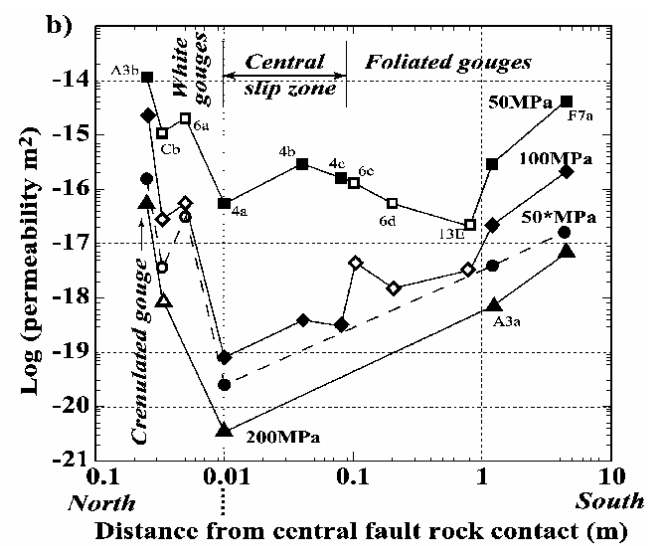

Median Tectonic Line (*Wibberley & Shimamoto.*, 2003)

Permeability Data of TCDP Siltstone (hole-A 837m)

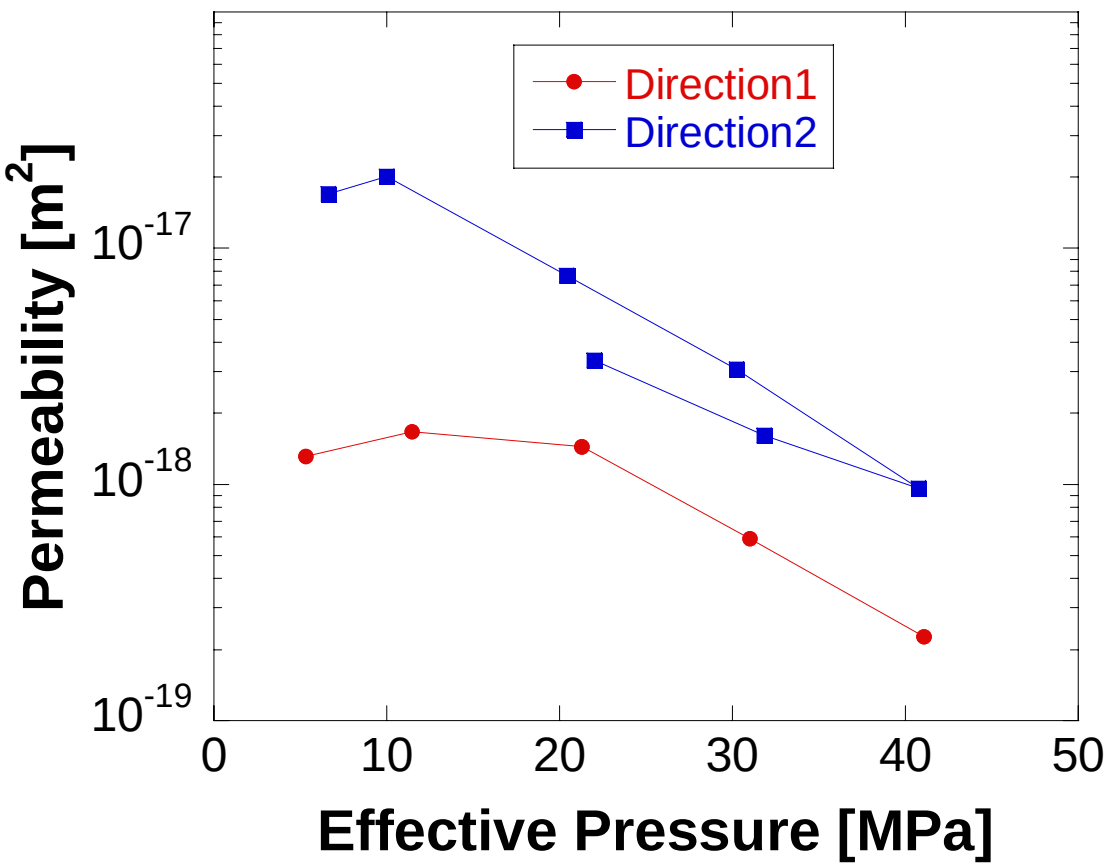

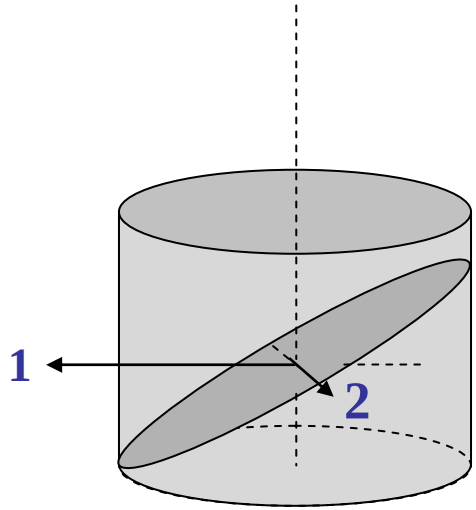

- Hydrostatic
- Low permeability
- An effective pressure of 35 MPa reduced the permeability by one order of magnitude

(*Chen et al.*, unpublished)

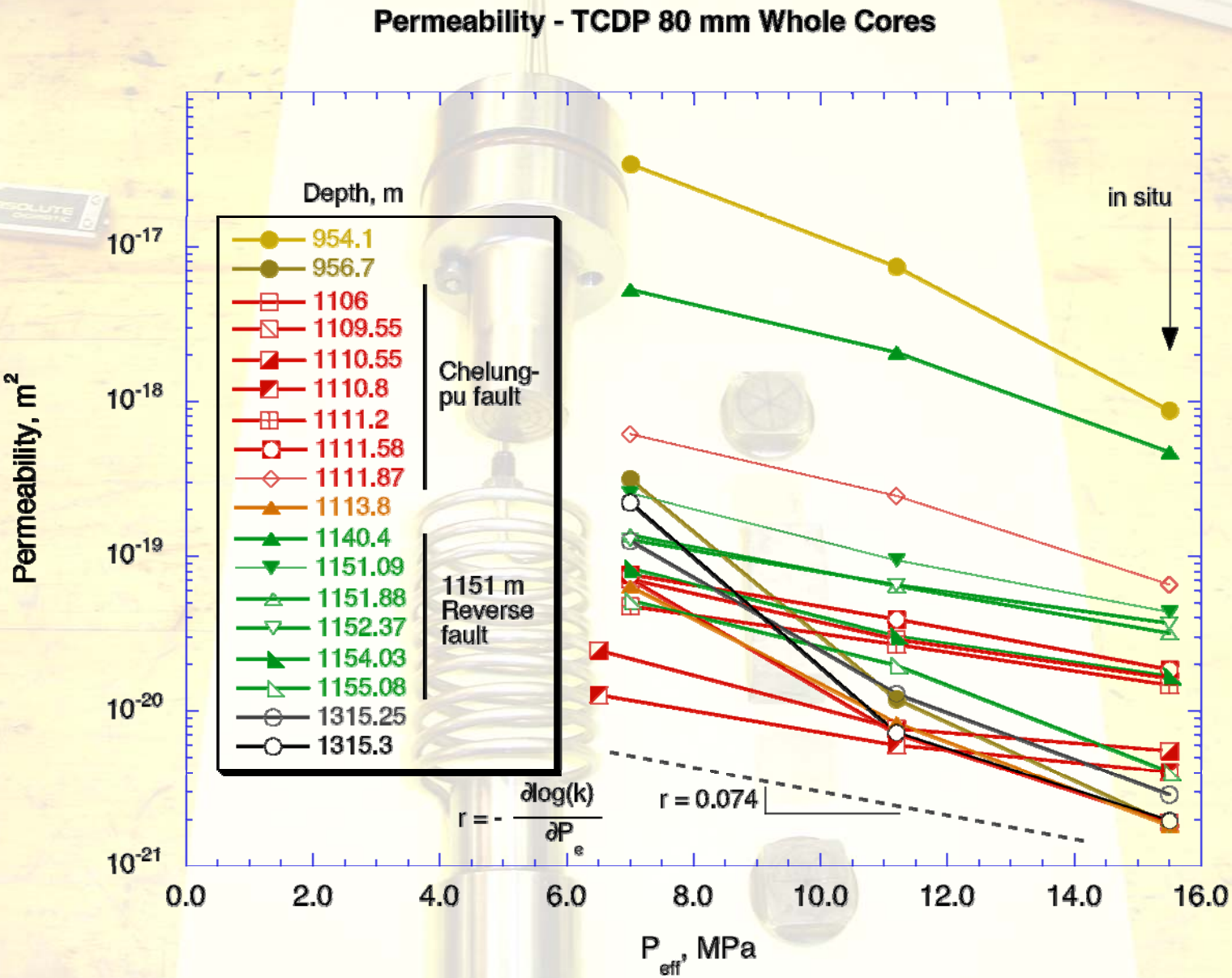

(*Morrow et al.*, unpublished)

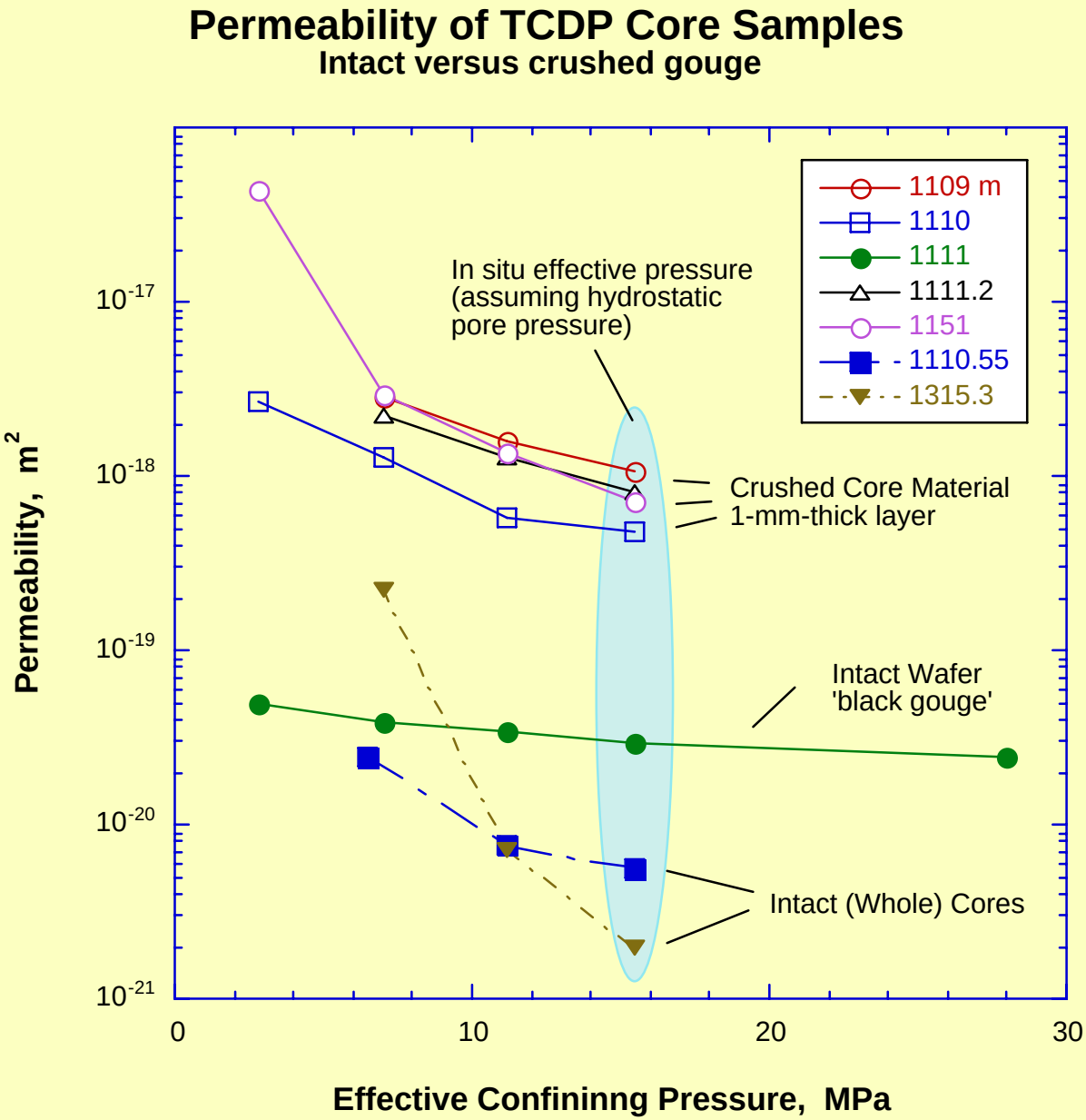
Permeability of TCDP Core Samples
Intact versus crushed gouge
1109 m
1110
1111
1111.2
1151
1110.55
1315.3
In situ effective pressure
(assuming hydrostatic
pore pressure)
Crushed Core Material
1-mm-thick layer
Intact Wafer
'black gouge'
Intact (Whole) Cores
Permeability, m2
10-17
10-18
10-19
10-20
10-21
0
10
20
30
Effective Confininng Pressure, MPa

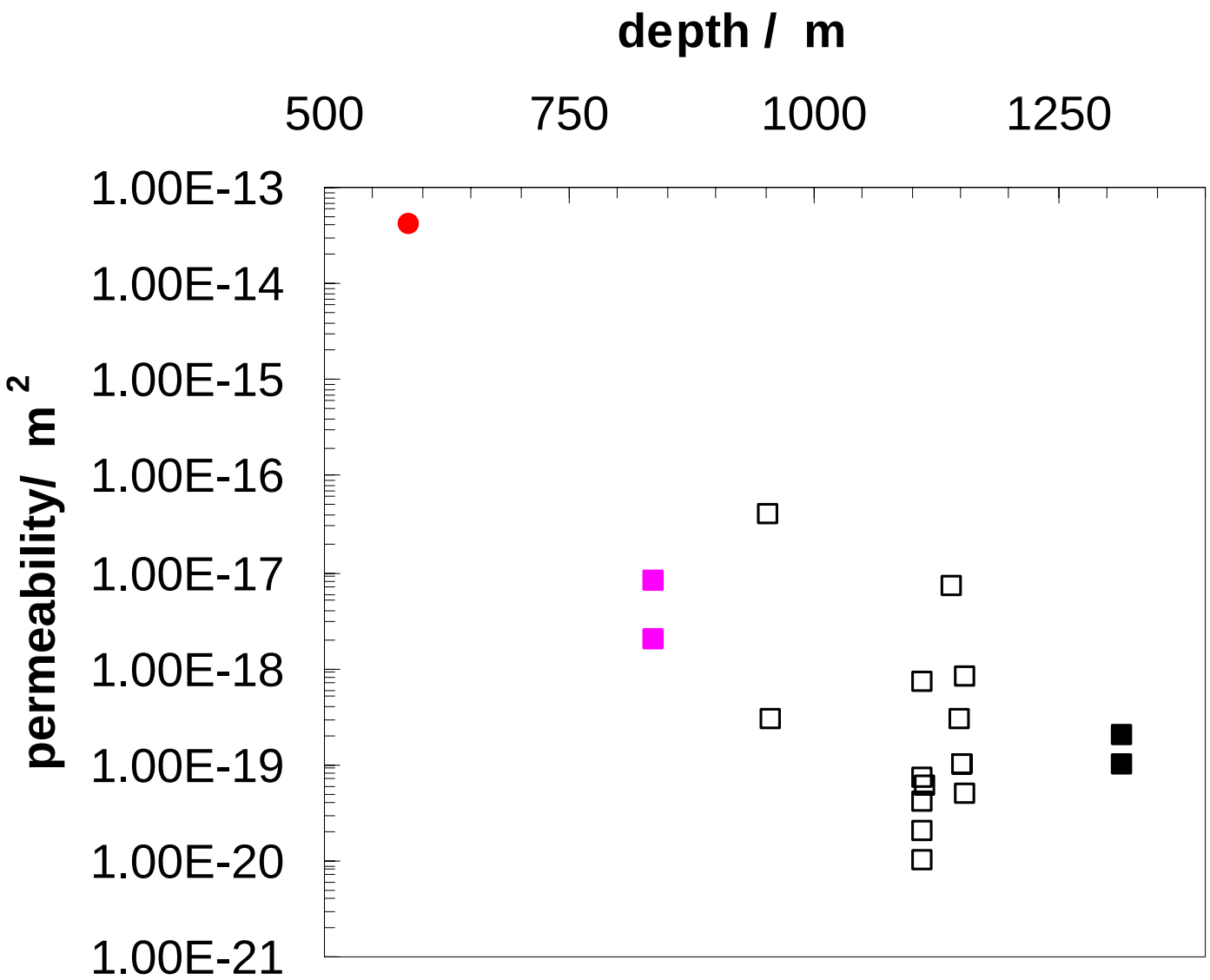

Summary of TCDP Permeability Data

Storativity of TCPD Whole Core Samples

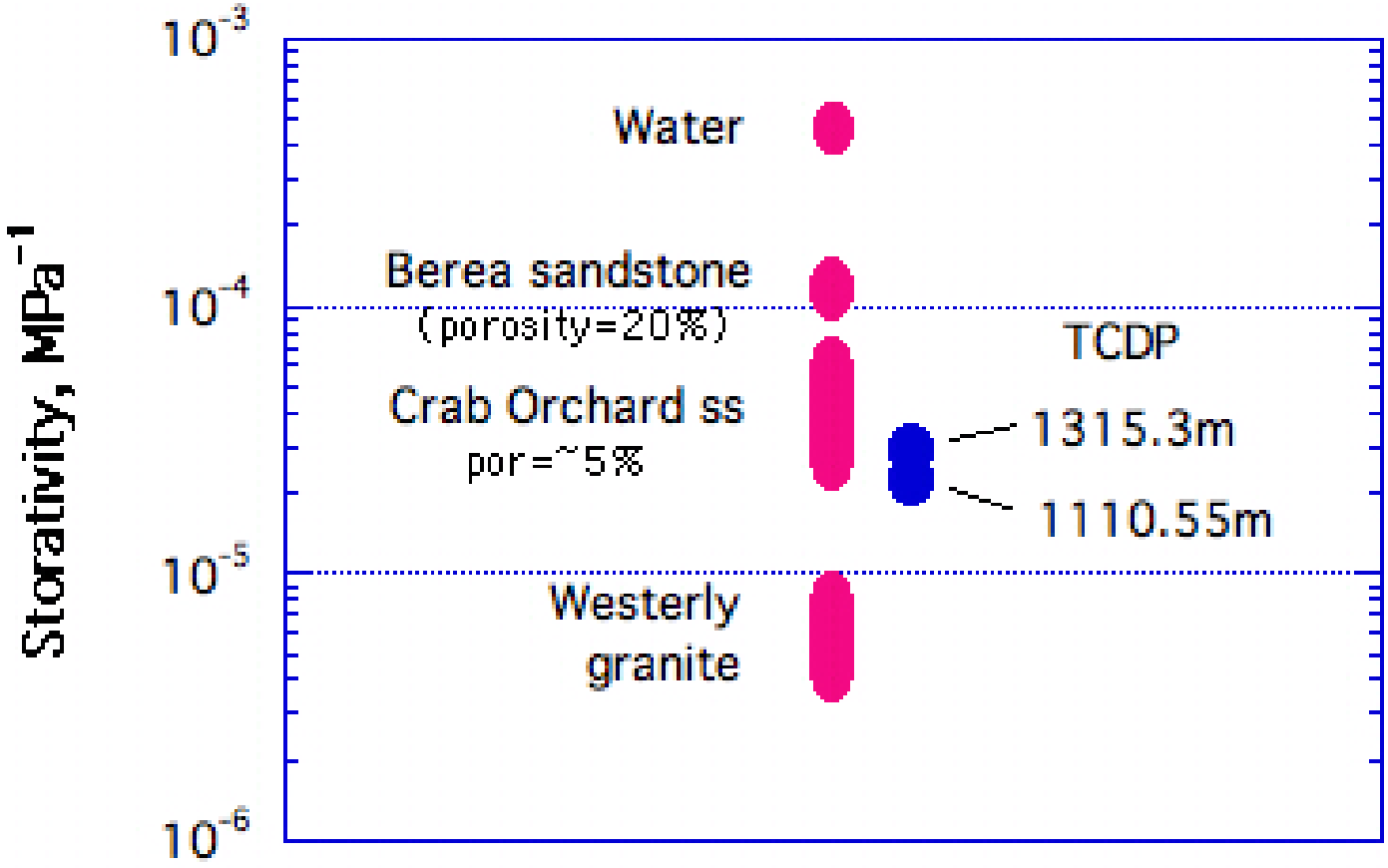

(*Morrow et al.*, unpublished)

Thermal Pressurization of Pore Fluid

- frictional heating due to seismic slip can raise the pore pressure, thus lowering the effective pressure and frictional strength (*Sibson*, 1973; *Lachenbruch*, 1980; *Mase and Smith*, 1987; *Lee and Delaney*, 1987)
- *Andrews* (2002) explicitly analyzed the consequence on stress drop during dynamic rupture

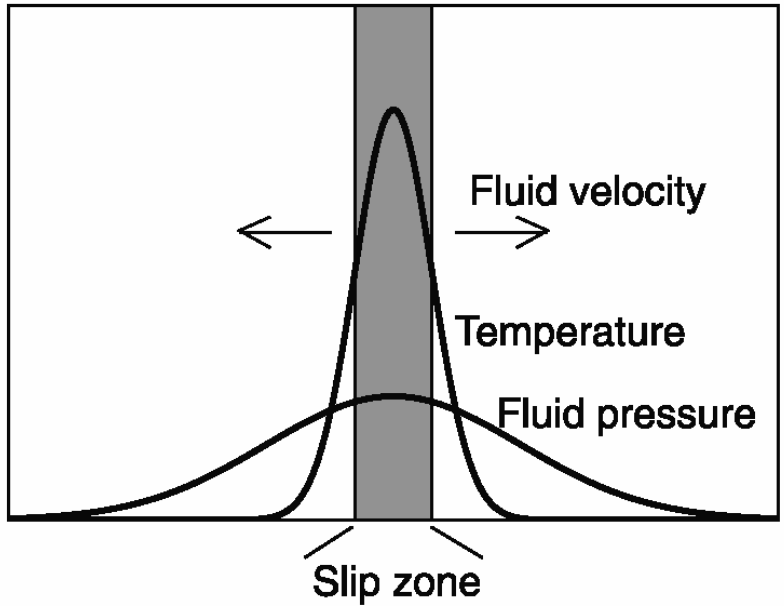

The frictional heat induces a pore pressure that scales with the *inverse square root* of hydraulic diffusivity ω times the elapsed time

$$P(t) - P_0 = \frac{\gamma}{\sqrt{2\pi}} \int_0^t \frac{\tau(t')v(t')\ dt'}{[2\omega(t-t') + D^2]^{1/2}}$$

$$\omega = \frac{K}{\phi\eta\beta}$$

$$\gamma = \frac{\alpha}{\beta c}$$

(contribution from the width D can effectively be taken to be 0)

Thermal Pressurization of Pore Fluid

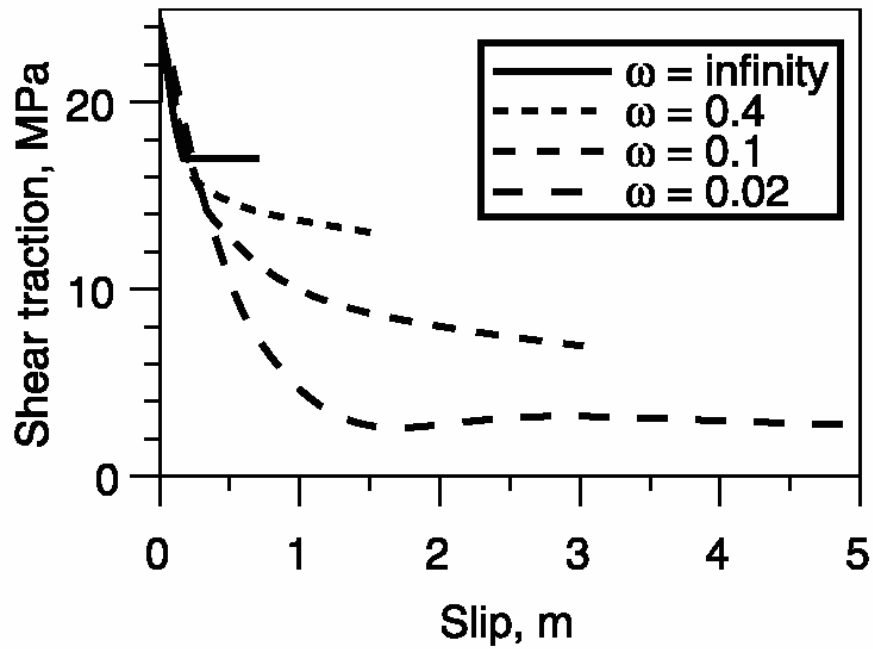

- stress drop increases with decreasing hydraulic diffusivity ω
- the slip-weakening behavior becomes *nonlinear*
- there is a threshold distance beyond which thermal pressurization dominates the stress drop process

$$R = \frac{8}{\pi} \frac{1}{(Cf\gamma)^2} \frac{\mu^2}{\tau^2} \frac{\omega}{v_R}$$

- if ω=0.02 m²/s, then *R*=300 m, which is comparable to the fault dimension of an earthquake with M=3.5
- the model neglects dilatancy and permeability evolution during the stress drop process.

permeability: $K = 5\ 10^{-17}\ \mathrm{m}^2$
porosity: $\phi = 0.025$
viscosity: $\eta = 10^{-4}$ Pa s
==> hydraulic diffusivity
$\omega = 0.02\ \mathrm{m}^2/\mathrm{s}$

$$\omega = \frac{K}{\phi\eta\beta}$$

Slip Distribution on Idealized Fault

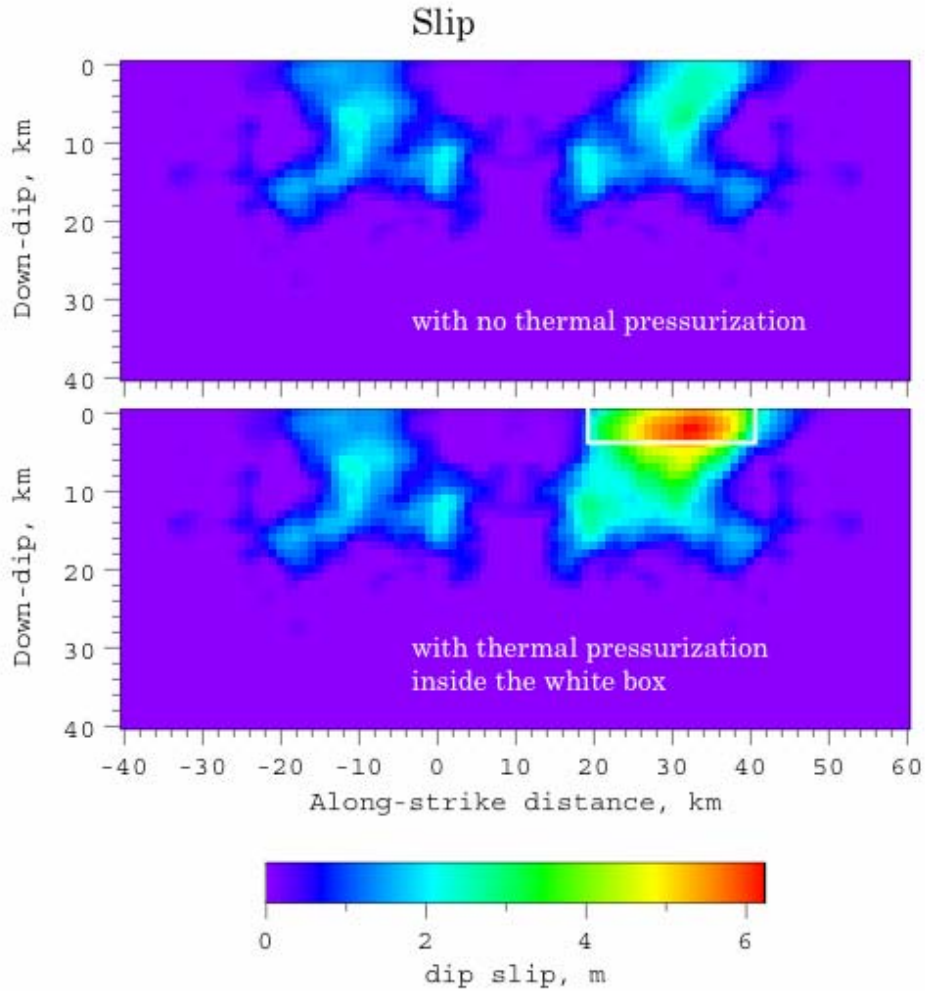

Andrews (May 2005)

In this calculation, a critical parameter is hydraulic diffusivity, ω, given by

$\omega = K/\eta S$

K = permeability
η = viscosity
S = Storage capacity.

	Value used in Andrews 2005	Values from TCPD Core Tests
f (coef. of frict.)	0.6	0.5 to 0.7
η [Pa-s]	10^{-4}	same
K [m^2]	2×10^{-17}	10^{-19} to 10^{-21}
S [Pa^{-1}]	2.5×10^{-11}	$\sim4\times10^{-11}$
ω [m^2/s]	0.02	2×10^{-6} to 2×10^{-5}

Conclusion: Hydraulic diffusivity in Chinshui shales is probably 3 orders of magnitude less than in Andrews' calculation.

What are the appropriate values for modeling poromechanical processes associated with dynamic rupture?

Heating and weakening of faults during earthquake slip

James R. Rice[1]

Received 21 August 2005; accepted 23 January 2006; published 24 May 2006.

[1] Field observations of mature crustal faults suggest that slip in individual events occurs primarily within a thin shear zone, <1–5 mm, within a finely granulated, ultracataclastic fault core. Relevant weakening processes in large crustal events are therefore suggested

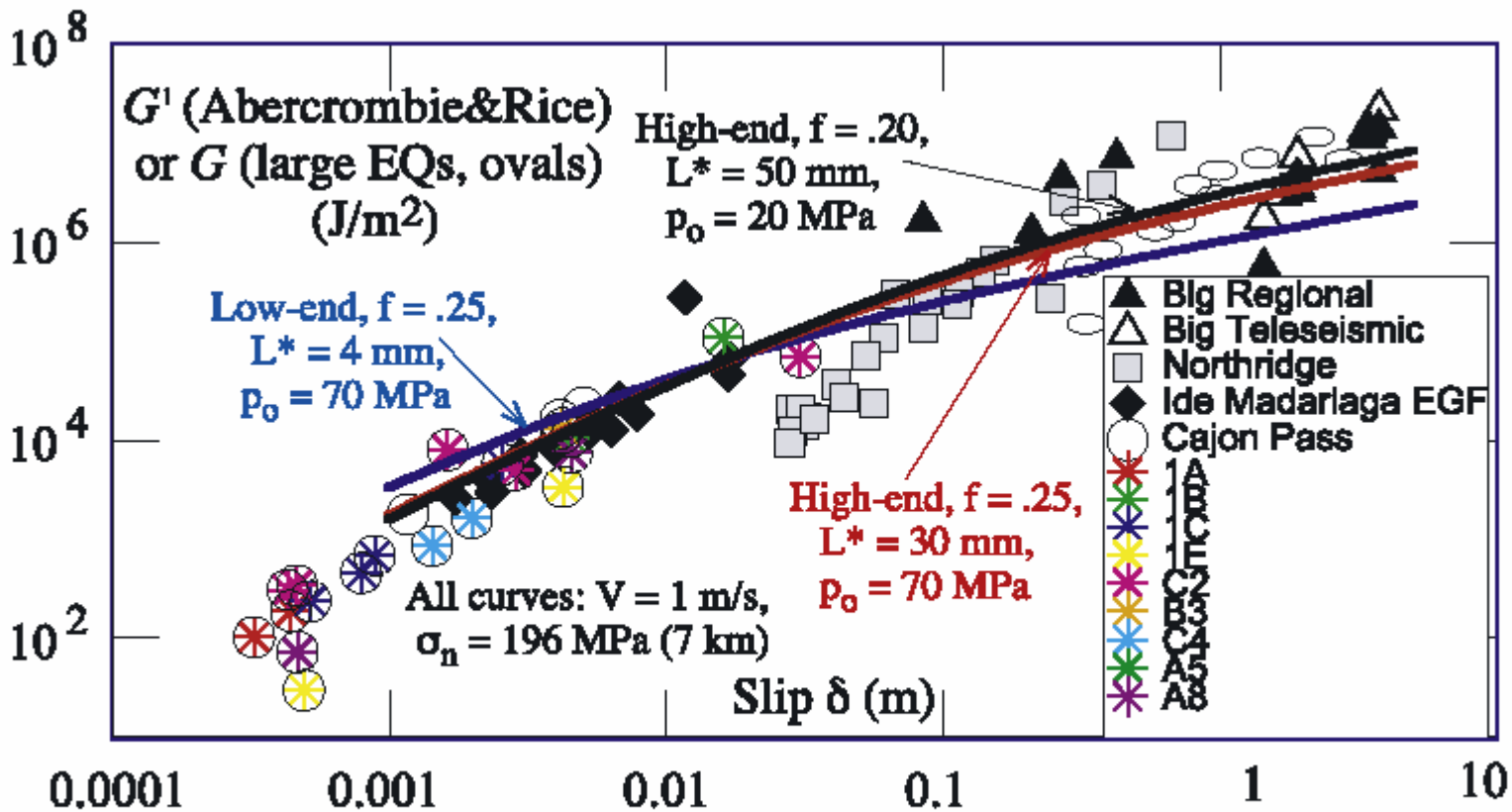

Figure 8. Lines show theoretical predictions of earthquake fracture energy G versus slip δ in the event, for the model of slip on a plane, based on combined effects of thermal pressurization of pore fluid and flash heating, with simplified representation assuming a constant friction coefficient f and slip rate V.

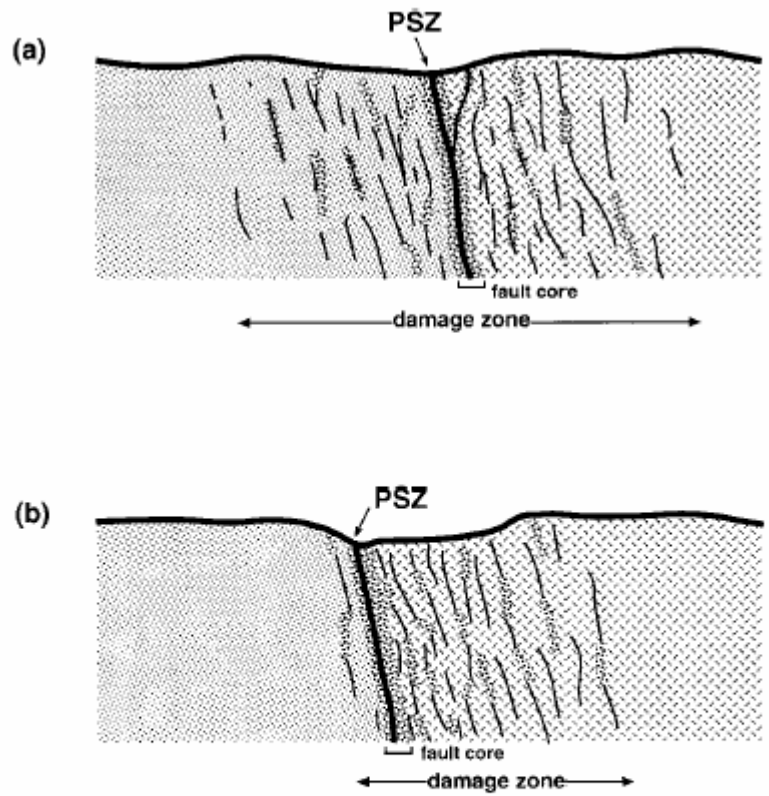

Figure 2. Schematic representations of brittle fault zones in the upper crust illustrating relationships of principal slip zone (PSZ), fault core, and damage zones: (a) approximately symmetric disposition; (b) PSZ localized at margin of damage zone. The coarse stipple denotes distributed cataclastic deformation and hydrothermal alteration of varying intensity, and lines represent subsidiary fractures.

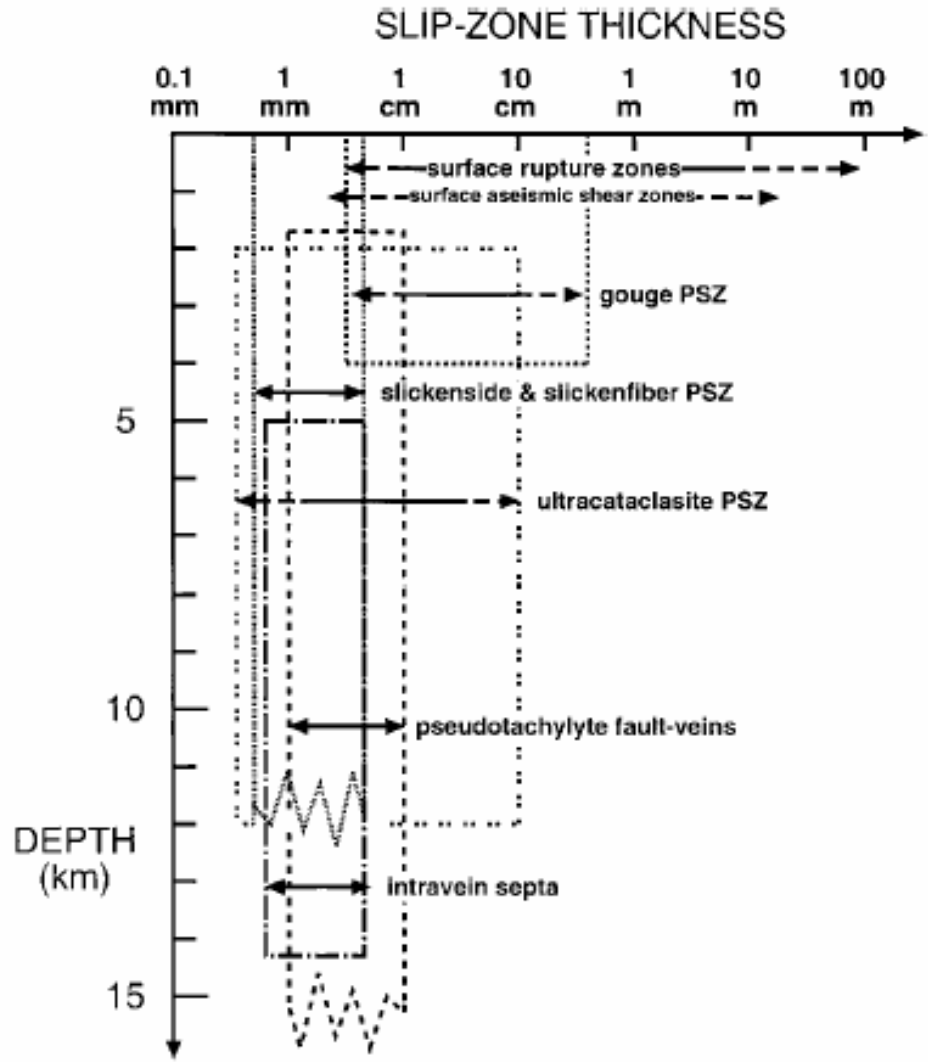

Figure 3. Geological estimates for the thickness of the seismic slip zone over various depth ranges as discussed in the text.

(*Sibson*., 2003)

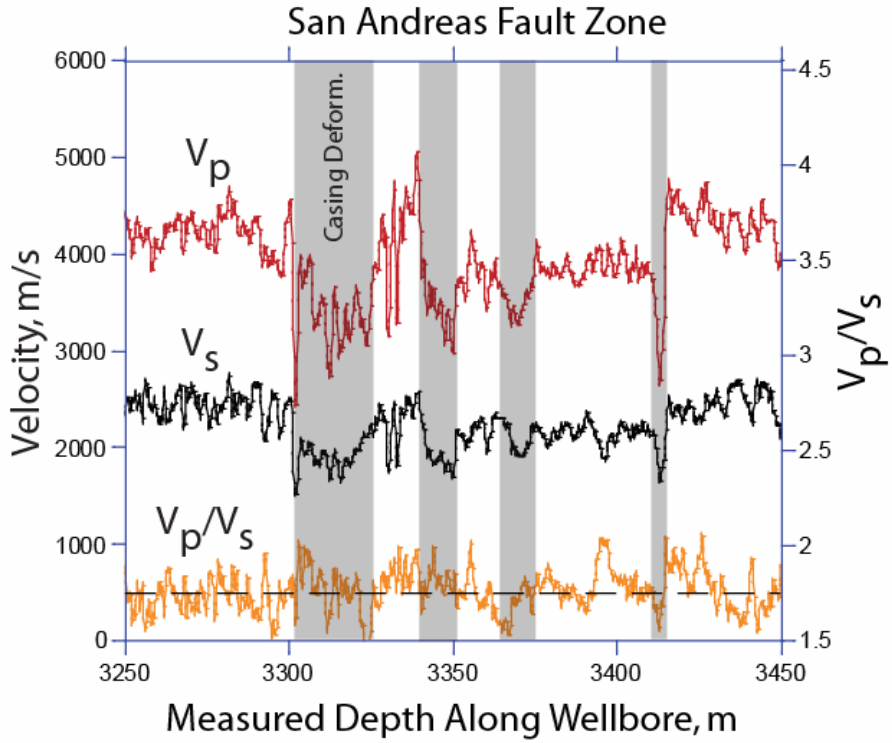

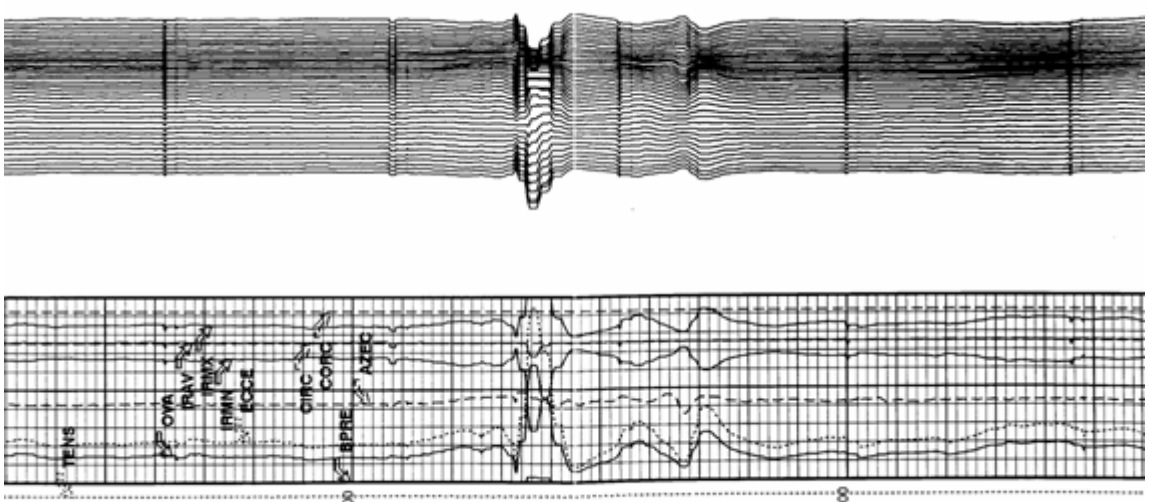

(*Zoback et al.*, AGU Fall Meeting, 2005)

Structure of Fault Cored at 3067 m MD
(*Almeida et al., this session*)

- Progressive increase in fracturing of siltstone toward fault core, and many of fracture surfaces contain slickensides
- Fault core contains sheared gouge layers (*white arrows*) and fault sliver of very fine grained sandstone
- Likely largest-displacement fault in spot cores acquired to date

Increase in deformation

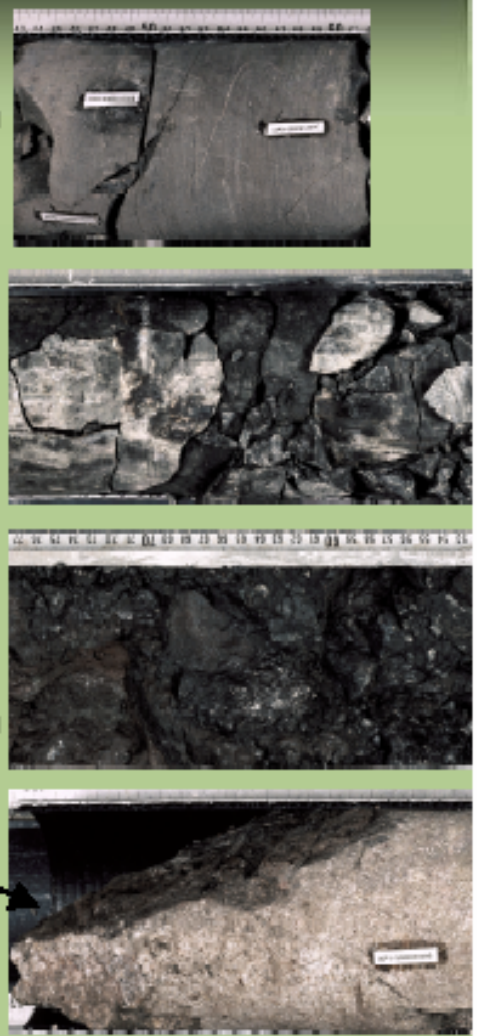

Fault surface

(AGU Fall Meeting, 2005)

TCDP Hole A - FZA1111

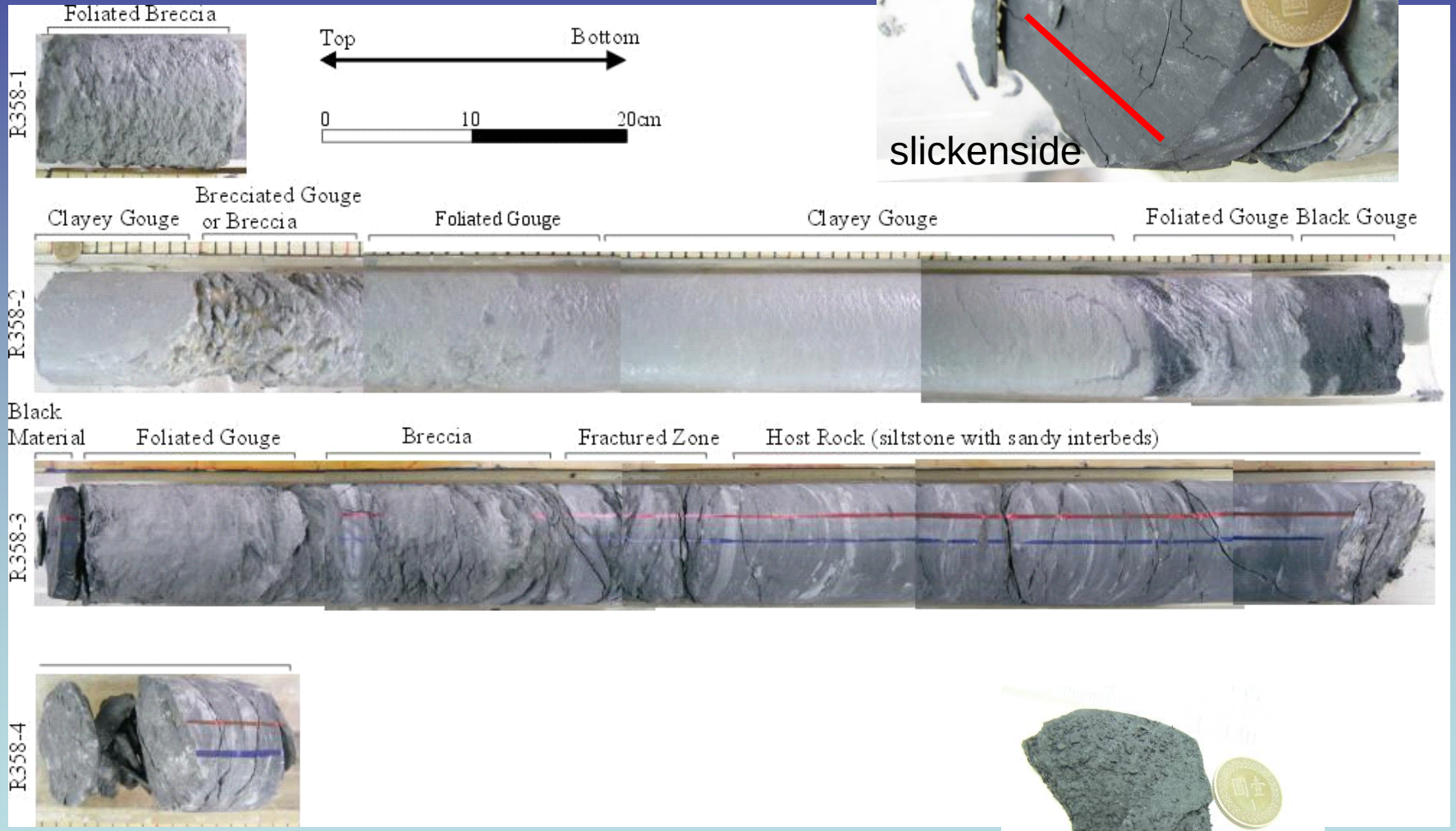

Black gouges in the Fault core of FZ1111

Décollement Zone: Sites 808 and 1174

- ~30 m thickness: 935-965 m depth
- Macroscopically, deformation is dominated by brittle fracture
- Increasing intensity of deformation down to abrupt base of fault zone
- Sharp contrast in physical properties across base of fault

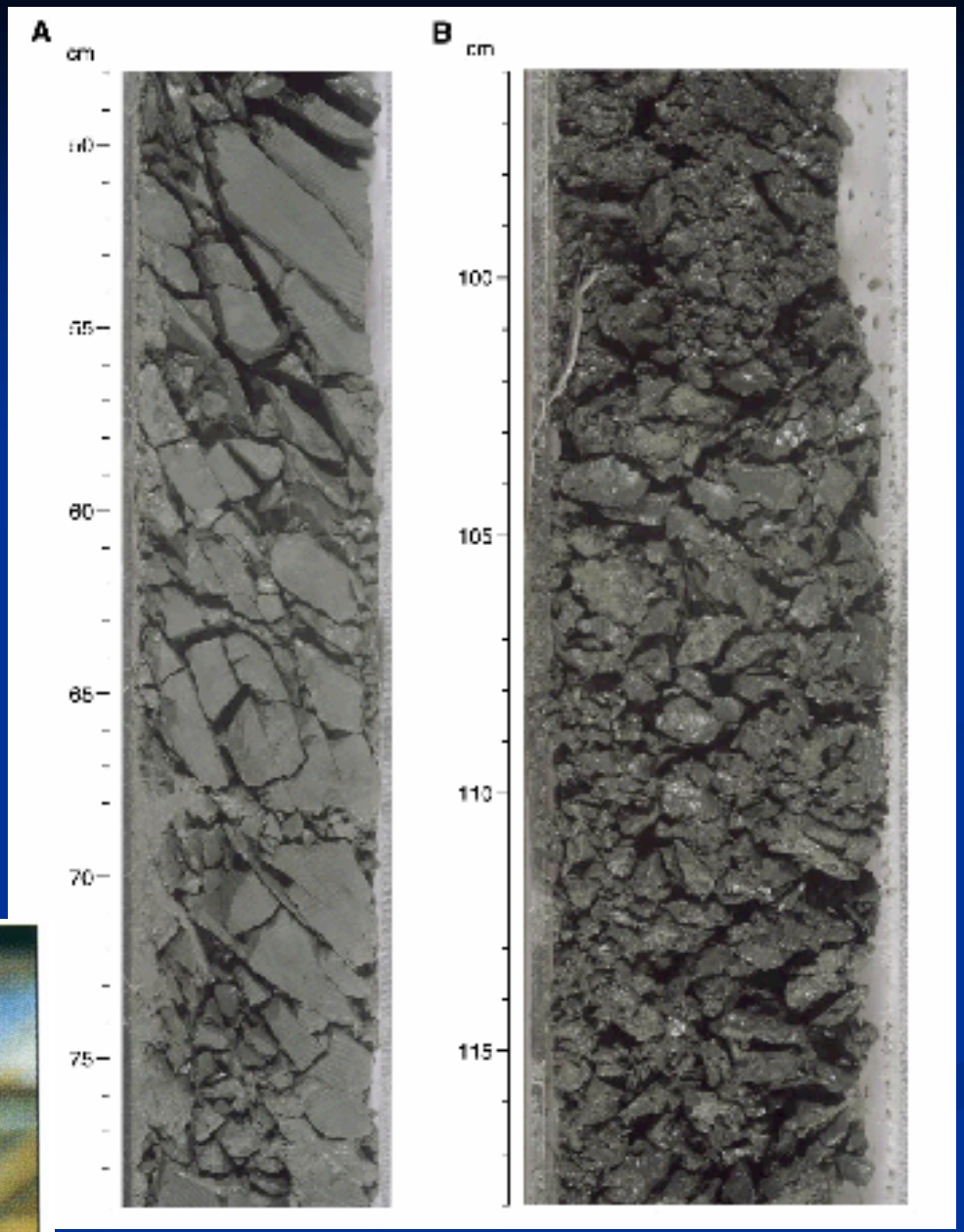

Décollement microstructures: upper brecciated domain

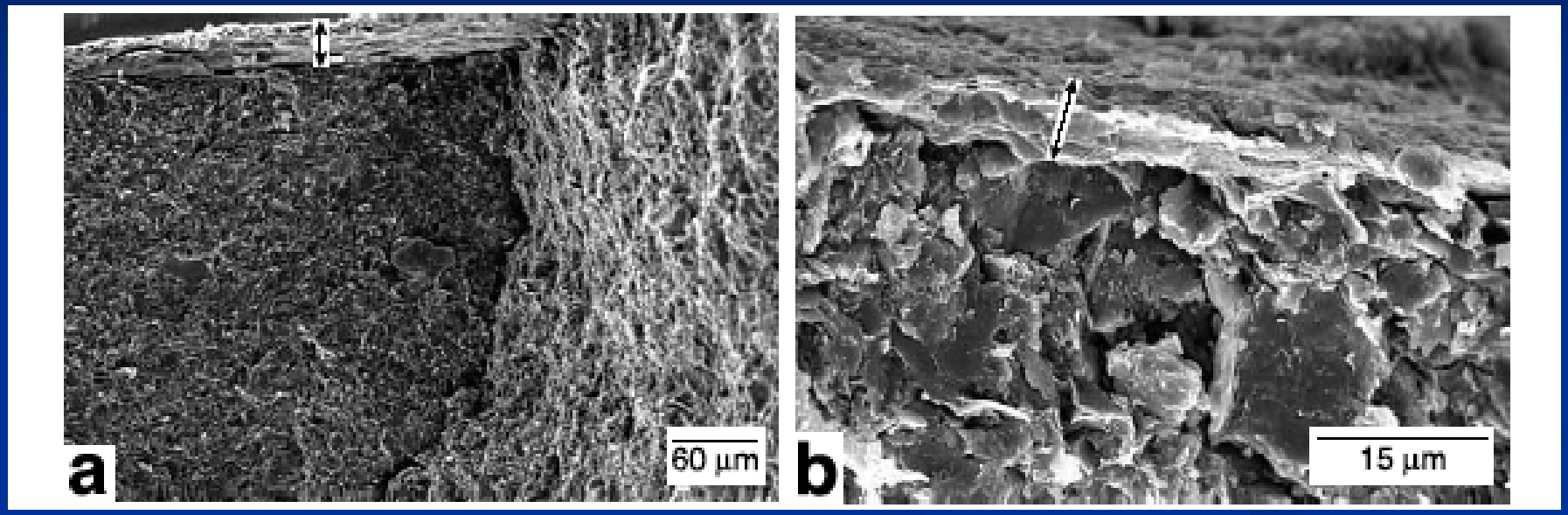

Ujiie et al., 2003 JGR

- Narrow shear zones of strongly aligned clay surround little-deformed blocks
- Block size decreases approaching the base of the fault zone --> shear strain increases

Nankai décollement microstructure: basal fault core zone

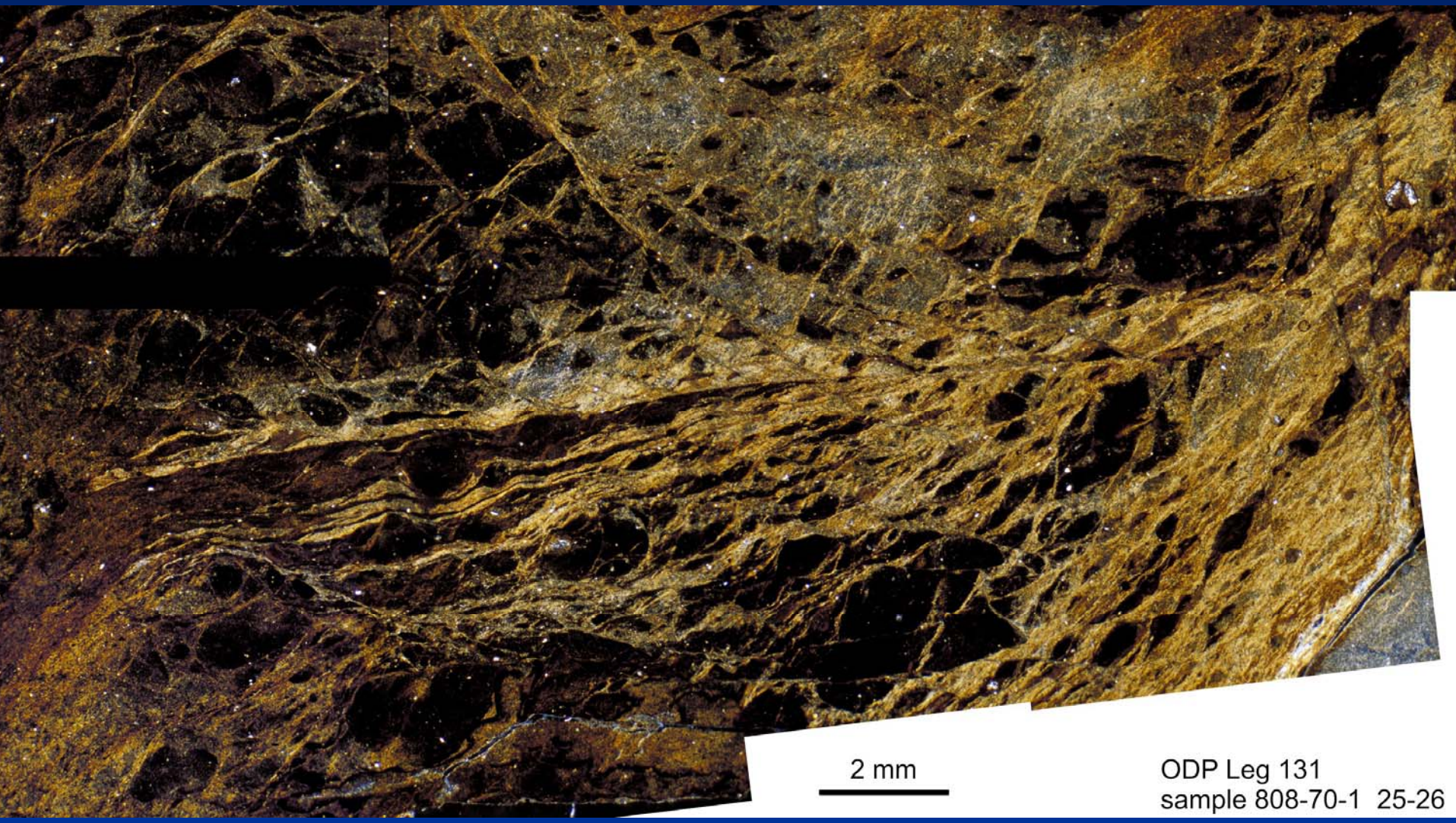

Vannucchi et al., 2003, JSG